FOI-R--1639--SE
May 2005
ISSN 1650-1942
Technical Report

Anders Larsson, Niklas Wingborg, Mattias Elfsberg and Patrik Appelgren

Characterization and electrical ignition of ADN-based liquid monopropellants

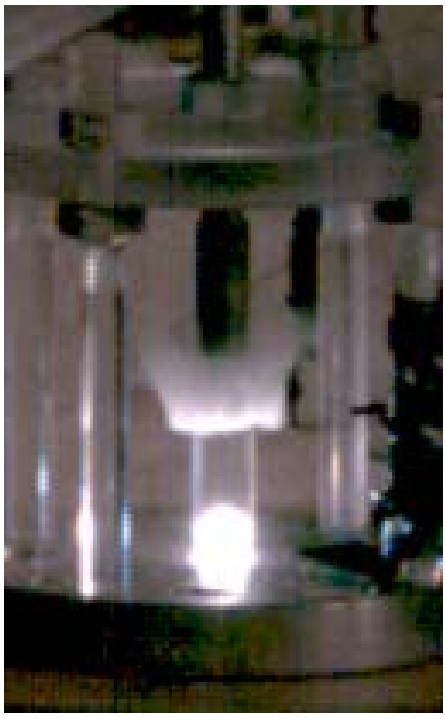

Weapons and Protection
SE-147 25 Tumba

SWEDISH DEFENCE RESEARCH AGENCY

Weapons and Protection
SE-147 25 Tumba

FOI-R--1639--SE

May 2005

ISSN 1650-1942

Technical Report

Anders Larsson, Niklas Wingborg, Mattias Elfsberg and Patrik Appelgren

Characterization and electrical ignition of ADN-based liquid monopropellants

Issuing organisation	Report number, ISRN	Report type
FOI – Swedish Defence Research Agency Weapons and Protection SE-147 25 Tumba	FOI-R--1639--SE	Technical Report
	Research area code 5. Strike and protection	
	Month year May 2005	**Project no.** I256
	Sub area code 51 Weapons and Protection	
	Sub area code 2	

Author/s (editor/s)	Project manager
Anders Larsson Niklas Wingborg Mattias Elfsberg Patrik Appelgren	Niklas Wingborg
	Approved by
	Sponsoring agency FOI Innovation Fund
	Scientifically and technically responsible

Report title

Characterization and electrical ignition of ADN-based liquid monopropellants

Abstract

Monopropellant hydrazine rockets are today widely used in missiles and spacecrafts. Hydrazine is however highly toxic, volatile and carcinogenic, and thus costly safety measures are required. During the last years there has been an increasing interest in Europe and in the USA to find a possible substitute, since a non-toxic monopropellant will offer substantial cost savings. ADN-based liquid monopropellants seems to be a promising alternative to hydrazine, being substantially easier to handle and having a 10 % higher specific impulse, and up to 60 % higher density-impulse, compared to hydrazine. To be able to replace hydrazine, ADN-based monopropellants must be as easy to ignite. Hydrazine and ADN-based liquid propellants are very different, and thus new ignition methods must be developed. This report presents the results from electrical ignition experiments of liquid ADN-propellants were the propellant is resistively heated by conducting an electric current through the propellant. It was found that substantially less electric energy was needed than expected. This is due to local phenomena close, or on the surface, of the electrodes. Very fast ignition was obtained, in most cases below 2 ms, and the lowest amount of electric energy needed was approximately 20 J. The pulsed-power supply required is estimated to weight of the order of one kilogram if getting the electric energy from the on-board electric power supply. These promising results show that this type of ignition method is feasible.

Keywords

ADN, monopropellant, ignition

Further bibliographic information	Language English
ISSN 1650-1942	**Pages** 49
	Price acc. to pricelist **Security classification**

Utgivare Totalförsvarets Forskningsinstitut - FOI Vapen och skydd 147 25 Tumba	**Rapportnummer, ISRN** FOI-R--1639--SE	**Klassificering** Teknisk rapport
	Forskningsområde 5. Bekämpning och skydd	
	Månad, år Maj 2005	**Projektnummer** I256
	Delområde 51 VVS med styrda vapen	
	Delområde 2	

Författare/redaktör Anders Larsson Niklas Wingborg Mattias Elfsberg Patrik Appelgren	**Projektledare** Niklas Wingborg
	Godkänd av
	Uppdragsgivare/kundbeteckning FOI Innovationsfond
	Tekniskt och/eller vetenskapligt ansvarig

Rapportens titel (i översättning)

Karaktärisering och elektrisk tändning av ADN-baserade flytande enkomponentsdrivämnen

Sammanfattning (högst 200 ord)

Hydrazin används idag som enkomponentsdrivämne i robotar och rymdfarkoster. Hydrazin är dock mycket giftigt, flyktigt och cancerogent, vilket gör det dyrbart att hantera. De senaste åren har intresset för alternativa ogiftiga drivämnen ökat, särskilt i Europa och i USA. Mindre giftiga drivämnen kan nämligen sänka hanteringskostnaderna avsevärt. Flytande ADN baserade enkomponentsdrivämnen verkar vara ett lovande alternativ, då dessa är betydligt lättare att hantera, har 10 % högre specifik impuls och upp till 60 % högre densitet-impuls. För att kunna ersätta hydrazin måste dock flytande ADN-drivämnen kunna antändas lika lätt. Hydrazin och flytande ADN-baserade drivämnen är mycket olika och därför måste nya antändningsmetoder utvecklas. Denna rapport presenterar resultaten från försök med elektrisk tändning av flytande ADN-drivämnen, där upphettning sker genom att leda en elektrisk ström genom drivämnet. Resultaten visar att det krävs betydligt mindre elektrisk energi än vad som förväntats. Detta beror på lokala effekter nära, eller på ytan av elektroderna. Tändningen var mycket snabb, i det flesta fallen under 2 ms, och den lägsta mängden elektrisk energi som krävdes var ca. 20 J. Vikten på pulskraftsaggregatet förväntas vara av storleksordningen ett kilogram om den elektriska energin kommer från farkostens ordinarie kraftaggregat. Dessa lovande resultat visar att denna typ av antändning är möjlig och rimlig.

Nyckelord

ADN, flytande drivämne, tändning

Övriga bibliografiska uppgifter	**Språk** Engelska
ISSN 1650-1942	**Antal sidor:** 49
Distribution enligt missiv	**Pris: Enligt prislista** **Sekretess**

Contents

Nomenclature

Symbol	Explanation	Unit
A	Area	m^2
a, b, c, d	Coefficients in equations 1 - 3	
C	Capacitance	F
c_p	Specific heat capacity	J/gK
h	Height	m
I	Current	A
I_{sp}	Specific impulse	Ns/kg
L	Inductance	H
m	Mass	kg
P	Power	W
R	Resistance	Ω
r	Radius	m
T_0	Initial sample temperature	°C
T_c	Combustion chamber temperature	°C
T_{min}	Minimum storage temperature	°C
t	Time	s
U	Voltage	V
V	Volume	m^3
W	Energy	J
ρ	Mass density	g/cm^3
σ	Electrical conductivity	S/m

1 Introduction

Rocket propulsion systems are widely used in missiles and spacecrafts. In some applications, it is desirable to be able to vary the thrust, or to have the possibility to switch-off and restart the propulsion system. Rocket propulsion systems that can provide this feature are hybrids, monopropellants, bipropellants and, to some extent, dual or multi pulse solid propellant rockets, or solid propellant rockets with variable nozzles. The advantage of using monopropellant systems are its simplicity and reliability. The specific impulse of monopropellants is, however, lower compared to bipropellants, but for small propulsion systems, monopropellants are competitive due to the compact design of the propulsion system, as seen in Figure 1.

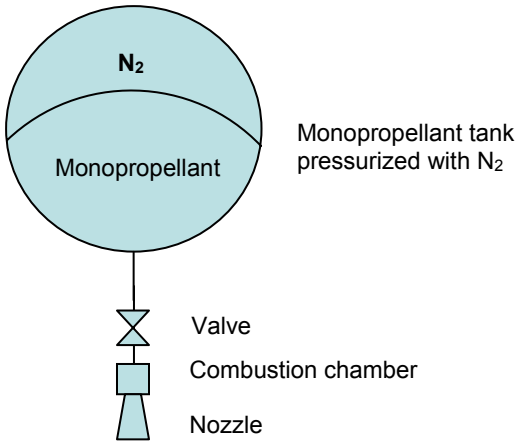

Figure 1. *Monopropellant propulsion system with "blow-down" feed system. The propellant and N_2 are separated by a rubber membrane.*

Hydrazine, N_2H_4, is today the most widely used monopropellant. The last years however, there has been a considerable interest in Europe and in the USA to find a possible substitute. The reason is the highly toxic nature of hydrazine, requiring costly safety measures during handling and testing. A non-toxic monopropellant is thus expected to offer substantial cost savings due to its ease of handling. Both ESA and NASA have identified advanced monopropellants as one of the most promising propulsion concepts of the future [1-6] and the development of new advanced monopropellants is today lead by the space sector.

One of the most promising alternatives to hydrazine is energetic ionic liquids based on an oxidizer salt dissolved in a hydrocarbon fuel/water mixture. This type of monopropellants is sometimes referred to as "green" monopropellants. As oxidizer salts, hydroxylammonium nitrates, HAN (NH_3OHNO_3) [3,5,7], ammonium dinitramide, ADN ($NH_4N(NO_2)_2$) [8-10], and hydrazinium nitroformate, HNF ($N_2H_5C(NO_2)_3$) [11-13], have received particular attention. Water is added to liquefy the propellant if the fuel is not able to dissolve all the oxidizer required. From a performance point of view, HAN and ADN are the most promising ones, due to their high solubility (95 and 78% respectively in water at 20°C [8,14]).

At the Swedish Defence Research Agency, FOI, the research on high performance "green" monopropellants have been focused on ADN-based formulations. Two promising fuels have been identified and propellants with them have been formulated. These two propellants are denoted FLP-105 (FOI Liquid Propellant number 105) and FLP-106 respectively. The

formulation and characterization of the propellants and the properties of ADN are described elsewhere [8,9,15-17] and their compositions are shown in Table 1. Table 2 shows their performance compared to hydrazine.

Table 1. Composition of propellant FLP-105 and FLP-106.

	FLP-105	FLP-106
ADN	65.7%	64.6%
Water	13.6%	23.9%
Fuel[a]	20.7%	11.5%

a) The fuels are described in reference [16] page 10-2.

Table 2. Comparison between hydrazine and FLP.

Propellant	Hydrazine[a]	FLP-105[b]	FLP-106[b]
ρ (g/cm^3) at 25°C	1.01	1.405	1.357
T_{min}[c] (°C)	+1	0	0
I_{sp} (Ns/kg)	2256 (230 s)	2560 (261 s)	2492 (254 s)
$\rho \cdot I_{sp}$ (Ns/dm^3)	2279	3597	3382
T_c (°C)	1100	1990	1814

a) Hydrazine data form reference [18].
b) FLP data from reference [9].
c) Minimum storage temperature determined by freezing (hydrazine) or precipitation (FLP).

As seen in Table 2, the specific impulse of the FLPs is approximately 10% higher compared to hydrazine. For small propulsion systems the density-impulse ($\rho \cdot I_{sp}$) is an important figure of merit. Due to the high density, the density-impulse for FLP-105 is approximately 60% higher compared to hydrazine.

One important aspect in the development of new monopropellant is the ignition. The state of the art hydrazine thrusters use catalytic ignition, which is reliable and simple. To replace hydrazine, ADN-based monopropellants must be as easy to ignite. One disadvantage with the ADN-based monopropellants is the high combustion temperature, which is 700 - 900°C higher compared to hydrazine. The current state of the art hydrazine catalyst (Shell 405) cannot withstand such high temperatures [5]. This and the fact that hydrazine and ADN-based liquid propellants are very different, both physically and chemically, require development of new ignition methods, or new catalysts.

When dripping the FLPs on a hot plate, with a temperature in the range of 200 to 250°C, they ignite and burn fast. This clearly shows that thermal ignition is possible. When running the samples in a differential scanning calorimeter, DSC, at a heating rate of 10 K/min, an exothermal reaction starts at approximately 150°C. This exothermal reaction correlates with the decomposition of ADN. Thus, the ignition temperature of the FLPs seems to be in the range of 150 to 200°C, depending on the test method and the heating rate. Three different methods of heating the propellant to the ignition temperature have been identified:

- Pyrotechnic (by forming hot gases using a solid energetic material which in turn will heat the propellant)
- Thermal conduction (by spraying the propellant on a hot object which in turn is heated by electric means)
- Resistive (ADN is a salt and thereby possesses a relatively high electric conductivity. This means that an ADN-based monopropellant can be resistively heated)

When using pyrotechnic ignition the number of ignitions will be equal to the number of pyrotechnic devices. Pyrotechnic ignition is thus not suitable for multi-pulse mode operations. In a missile or a satellite the amount of electric energy available are limited. In both thermal conduction ignition and resistive ignition, electric energy is the main energy source. Heating the propellant by thermal conduction will require more electric energy compared to resistive heating since, in the latter case, only the propellants itself needs to be heated. Thus, the latter is to prefer. This work is concentrated upon an investigation about the possibilities of resistive ignition of ADN-based monopropellants. Some of the physical properties of the monopropellants have previously been characterized [9]. To be able to calculate the energy needed and to model the ignition, the characterization has been complemented by measuring the electric conductivity, the mass density, and the specific heat capacity, as functions of temperature.

2 Characterization of the ADN-based monopropellants

The characterization of the ADN-based monopropellants in this study has been focused on electric conductivity, mass density, and specific heat capacity, as functions of temperature. The mass density has previously been measured on FLP-105 and FLP-106 between 5 and 60°C [9]. In this study, it was however desired to characterize the needed physical properties up to at least 80°C.

2.1 Experimental methods

The specific heat capacity measurements were performed using a Mettler Toledo DSC30 with liquid nitrogen cooling. The measuring cell was purged with nitrogen (50 ml/min) and the temperature was adjusted using a two-point calibration with indium (Mettler calibration standard) and HPLC-grade water. The heat flow was calibrated by running four samples of HPLC-grade water from 0 to 100°C and the results were then adjusted to literature data between 20 and 100°C [19]. Below 20°C the results showed initial deviation due to thermal inertia of the DSC. Measurements with empty cups were conducted first to ensure that any differences between the heat capacity of the cups were accounted for. All samples were put in sealed aluminium cups to prevent evaporation. The mass of the samples was in the range of 30 to 50 mg.

A Mettler Toledo DE40 density meter was used to determine the mass density of the propellants. Calibration was done using HPLC-grade water. All reported densities are the average of at least two measurements.

The electrical conductivity was measured using a WTW inoLab 720 precision conductivity meter, equipped with a TetraCon 325 standard conductivity cell. The cell constant was calibrated using a 0.01 mol/l KCl control standard (Radiometer analytical KS920, 0.1413 S/m at 25°C) and the temperature was controlled using a thermostat bath. To check the calibration at higher conductivity values, and at different temperatures, a Reagecon CSKC200M (20 S/m at 25°C) conductive standard was used. The measured values were slightly higher than stated by the standard (+0.6%) and the values were accordingly adjusted. All reported values are an average of two measurements.

2.2 Results

2.2.1 Specific heat capacity

The calibration of the measurement instrument was checked using diethylene glycol. The measured value at 25.0°C (2.32 J/gK) correlated well with literature data (2.31 J/gK) [19]. Figure 2 shows the results from two measurements on FLP-105 and FLP-106 respectively. The calibration curve with water and the corresponding literature data at different temperatures are also shown.

The specific heat capacity of FLP-106 is higher compared to FLP-105. This is likely due to the higher water content in FLP-106. A linear equation, (1), was fitted to the experimental data in Figure 2. The values of the coefficients in (1) are shown in Table 2. Temperature values in (1) are in degrees Celsius.

$$c_p = c_{p0} + aT \qquad (1)$$

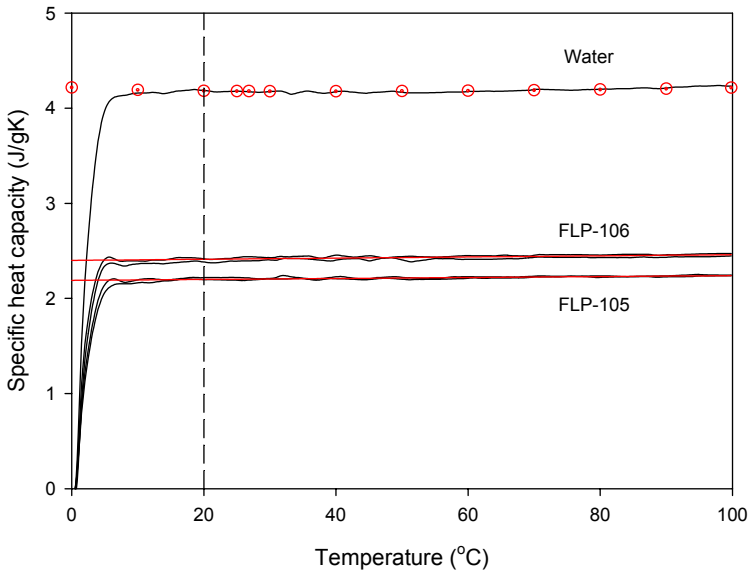

Figure 2. *Specific heat capacity as a function of temperature. Below 20°C the measurements shows initial deviation due to thermal inertia of the instrument.*

Table 3. Coefficients in (1) for calculating the specific heat capacity, c_p (J/gK).

	c_{p0}[a] (J/gK)	a (J/gK^2)	Measured c_p (J/gK) at 25°C
FLP-105	2.19	$5 \cdot 10^{-4}$	2.21
FLP-106	2.40	$6 \cdot 10^{-4}$	2.41

a) c_{p0} = extrapolated specific heat capacity at 0°C.

2.2.2 Mass density

Figure 3 shows the measured densities of FLP-105 and FLP-106 at temperatures from 5 to 80°C. As seen in Figure 3, the mass density varies linearly with the temperature and can thus be calculated according to (2). The higher mass density of FLP-105 is linked to its higher content of ADN, compared to FLP-106.

$$\rho = \rho_0 + bT \qquad (2)$$

By linear regression the coefficients in (2) were fitted to the experimental data in Figure 3, showing excellent correlation (r^2>0.9999) for both FLP-105 and FLP-106. The results are shown in Table 4. Temperature values in (2) are in degrees Celsius.

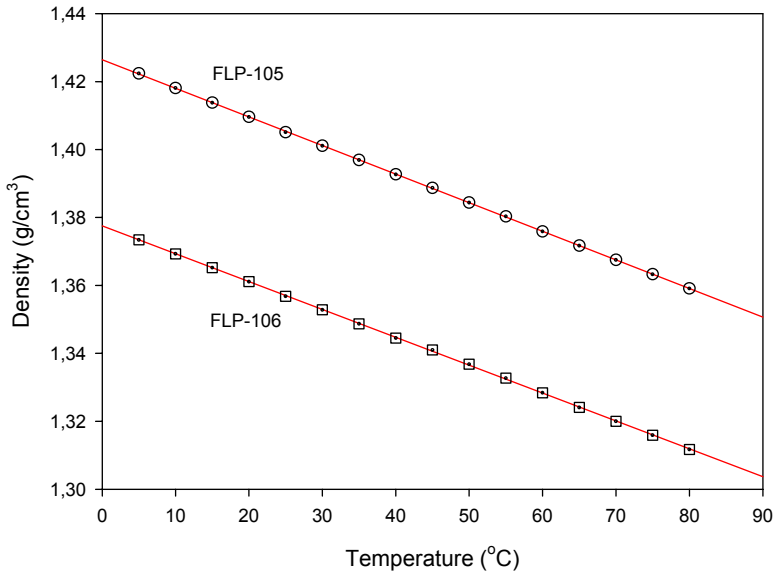

Figure 3. *Mass density as a function of temperature.*

Table 4. Coefficients in (2) for calculating the mass density ρ (g/cm^3).

	ρ_0[a] (g/cm^3)	b (g/Kcm^3)	Measured ρ (g/cm^3) at 25°C
FLP-105	1.426	$-8.4\cdot10^{-4}$	1.405
FLP-106	1.378	$-8.2\cdot10^{-4}$	1.357

a) ρ_0 = extrapolated mass density at 0°C.

2.2.3 *Electric conductivity*

Figure 4 shows the results from the measurements of the electric conductivity in FLP-105 and FLP-106 at temperatures between 5 and 80°C. The results in Figure 4 do not follow a linear relation, and thus a second order polynomial, (3), was fitted to the experimental data. The results are shown in Table 5. Temperature values in (3) are in degrees Celsius.

$$\sigma = \sigma_0 + cT + dT^2 \qquad (3)$$

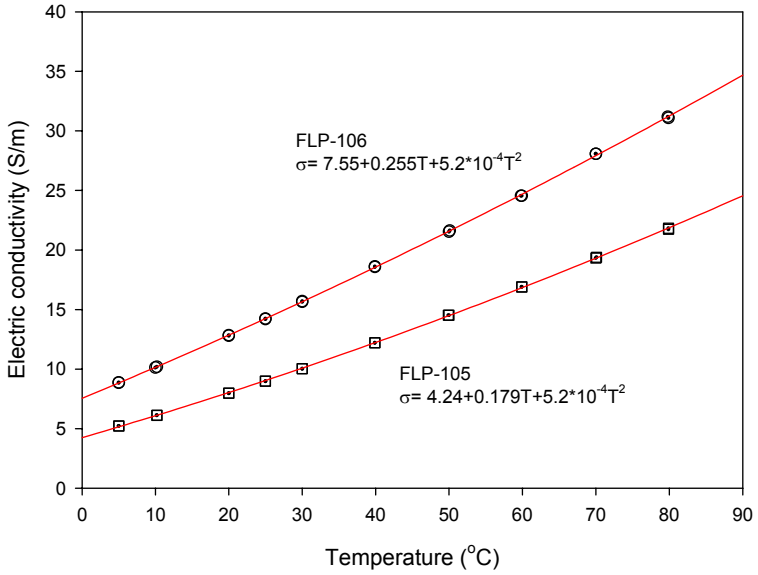

Figure 4. *Electrical conductivity as a function of temperature.*

Table 5. Coefficients in (3) for calculating the electric conductivity, σ (S/m).

	σ_0[a] (S/m)	c (S/Km)	d (S/K^{2}m)	Measured σ at 25°C (S/m)
FLP-105	4.24	0.179	$5.2\cdot10^{-4}$	9.0
FLP-106	7.55	0.255	$5.2\cdot10^{-4}$	14.2

a) σ_0 = extrapolated electric conductivity at 0°C.

2.3 Summary from the monopropellant characterization

Table 6 summarizes the results from the monopropellant characterization work. These data were used in the following section.

Table 6. Propellant properties as a function of temperature. All temperatures in °C.

Monopropellant:	FLP-105	FLP-106
Mass density, ρ (g/cm^3)	$1.426-8.4\cdot10^{-4}$T	$1.378-8.2\cdot10^{-4}$T
Specific heat capacity, c_p (J/gK)	$2.19+5\cdot10^{-4}$T	$2.40+6\cdot10^{-4}$T
Conductivity, σ (S/m)	$4.24+0.179T+5.2\cdot10^{-4}T^2$	$7.55+0.255T+5.2\cdot10^{-4}T^2$

3 Preparatory Analysis

The equivalent electric circuit of the test set-up is shown in Figure 5. A detailed description of the experimental arrangement is given in Section 4. The pulsed-power supply and the connecting wires are represented by the *RLC*-elements with the following values: R = 30 mΩ, L = 1.1 μH and C = 67 μF. The propellant sample is the load, which is designated R_L. The propellant sample is heated by the current and thereby its resistance varies in time.

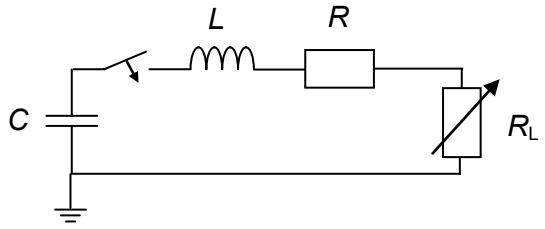

Figure 5. *The equivalent electric circuit of the test set-up. The RLC-components are the capacitance, the inductance and the resistance of the pulsed-power supply and its connections. R_L is the resistance of the propellant sample.*

3.1 Modelling sample temperature and sample resistance

The temperature and the resistance of the sample are estimated by the following analysis. The volume of the sample is a cylinder with radius r and height h. Thus, its cross-sectional area is $A = \pi r^2$ and its volume is $V = \pi r^2 h$. The resistance R of the sample in the axial direction is given by

$$R = \frac{h}{\sigma(T)A} \tag{4}$$

where $\sigma(T)$ is the temperature-dependent electrical conductivity of the sample material given by Table 6. The temperature increase of the sample is given by the resistive heating of it. The momentary dissipated electrical energy dW is given by

$$\mathrm{d}W = UI\mathrm{d}t \tag{5}$$

where U is the voltage across, and I the current trough, the sample. If neglecting heat losses, all this energy contributes to the temperature increase dT according to

$$\mathrm{d}W = c_\mathrm{p}(T)m\mathrm{d}T \tag{6}$$

where $c_\mathrm{p}(T)$ is the temperature-dependent specific heat capacity of the sample material and m is its mass. Thus, integration of the differential equation

$$\frac{\mathrm{d}T}{\mathrm{d}t} = \frac{UI}{c_\mathrm{p}(T)m} \tag{7}$$

gives the temperature of the sample, given the initial temperature $T(t{=}0) = T_0$. The specific heat capacity is a material property and is given by Table 6. The mass is given as the product of the volume and the mass density at the initial time according to

$$m = \rho(T_0)V \tag{8}$$

where the mass density is given by Table 6. Note that the model does not include any chemical reactions in the sample. Such reactions might increase the sample temperature.

3.2 Numerical simulations

The circuit equation of Figure 5 is solved with the variable load resistance according to (4) and the temperature is given by solving (7). The typical output of a simulation is shown in Figures 6-8. The simulation parameters were:

- Propellant: FPL-105
- Initial temperature: 20 ºC
- Sample radius: 4.5 mm
- Sample height: 25 mm
- Applied voltage: 5 kV

Figure 6 shows the development in time of the voltage across, and the current through, the sample together with the sample temperature. The sample resistance is shown in Figure 7, and the power and dissipated energy is shown in Figure 8. The sequence of events is that when the electric energy of the capacitor in the pulsed-power supply is discharged through the sample, a current is flowing through the sample and the voltage across it decreases. The current causes ohmic heating of the sample, resulting in a temperature increase. Since the electrical conductivity of the propellant is increasing with temperature, the resistance of the sample decreases and the current is initially increasing. Nevertheless, since the voltage is decreasing, the current exhibits a maximum before all the energy of the pulsed-power supply is discharged. The calculations show that the current peaks around a few hundreds amperes, the duration of the discharge is a few milliseconds and the final temperature of the propellant is about 190 °C.

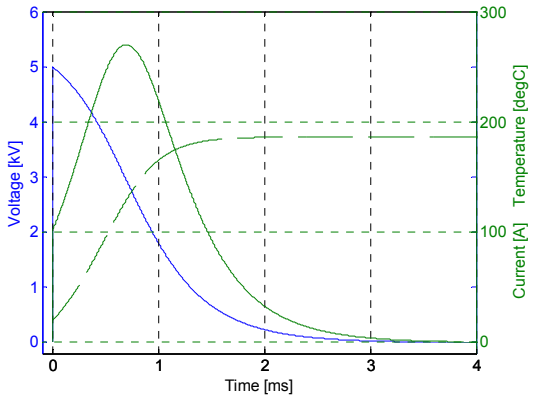

Figure 6. *Numerical simulation of the voltage across, and the current through the propellant sample together with the sample temperature. The solid line is the current and the dashed line is the temperature. The conditions for the simulations were a sample of FLP-105 with an initial temperature of 20 ºC and with a radius of 4.5 mm and a height of 25 mm. The applied voltage was 5 kV.*

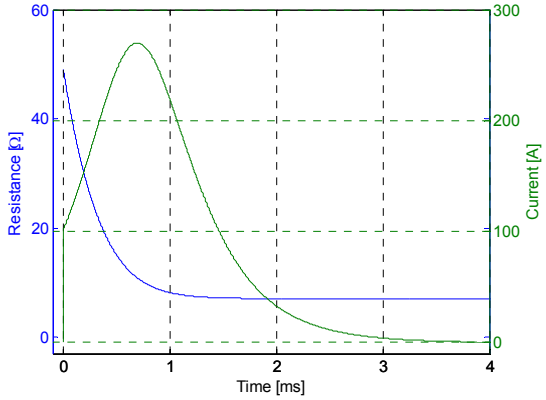

Figure 7. *The resistance of the sample together with the current through the sample. Conditions as in Figure 6.*

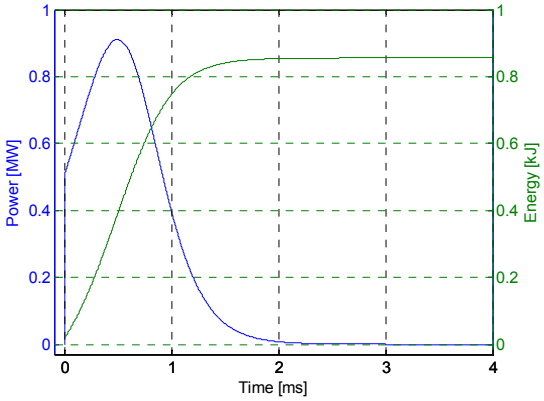

Figure 8. *The power consumed in the sample and the accumulated energy. Conditions as in Figure 6.*

Several parameters can be varied in the simulations. For instance, Figure 9 shows the sample temperature for different propellants. Since FLP-106 has a higher conductivity than FLP-105, the temperature increase is slightly faster and since FLP-106 has a lower specific heat capacity, the total temperature increase is slightly lower.

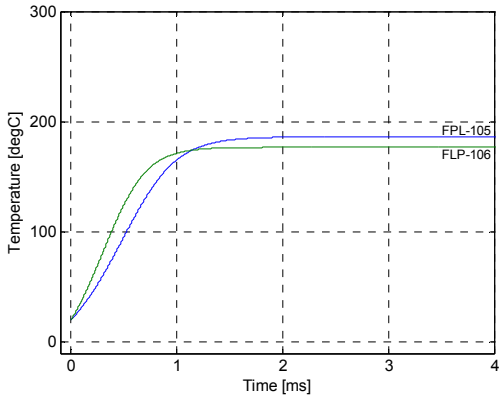

Figure 9. *The temperature of the sample for different propellants. Other conditions are the same as in Figures 6-8.*

The main hypothesis is to increase the temperature of the sample to its ignition temperature. Figure 10 shows the development in time of the sample temperature with the voltage of the pulsed-power supply as a parameter. The horizontal line in the graph, at the temperature of 150 °C, indicates the lower limit of the estimated ignition temperature, as determined by DSC measurements. This limit temperature is reached for an applied voltage of 5 kV and higher, but not for an applied voltage of 4 kV and lower. One may infer that an applied voltage of about 4.5 kV is the minimum requirement for reaching the ignition temperature. A voltage of 4.5 kV is here equivalent to a stored electric energy of $W = CU^2/2 = 0.68$ kJ.

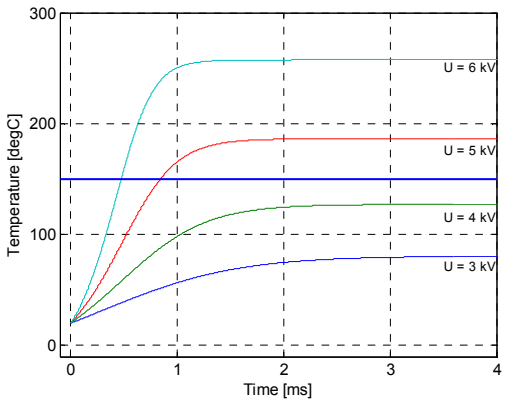

Figure 10. *The temperature of the propellant for different values of the applied voltage. Other conditions are the same as in Figure 6-8. The horizontal line indicates the estimate of the lower limit of ignition temperature of 150 °C.*

3.3 Conclusions from simulations

With the used pulsed-power supply and sample sizes indicated above, the simulations give the following properties of the circuit:

- The current through the sample is a few hundreds amperes.
- The pulsed-power supply is discharged in a few milliseconds.
- To reach ignition temperature, the pulsed-power supply has to be charged to about 4 - 5 kV.

4 Experimental Arrangement

4.1 Test set-up

An experiment arrangement for the electrical ignition of the liquid propellant was designed and constructed. Figure 11 shows a schematic picture of the experiment arrangement with the pulsed-power supply, sample holder, anode, cathode and diagnostics.

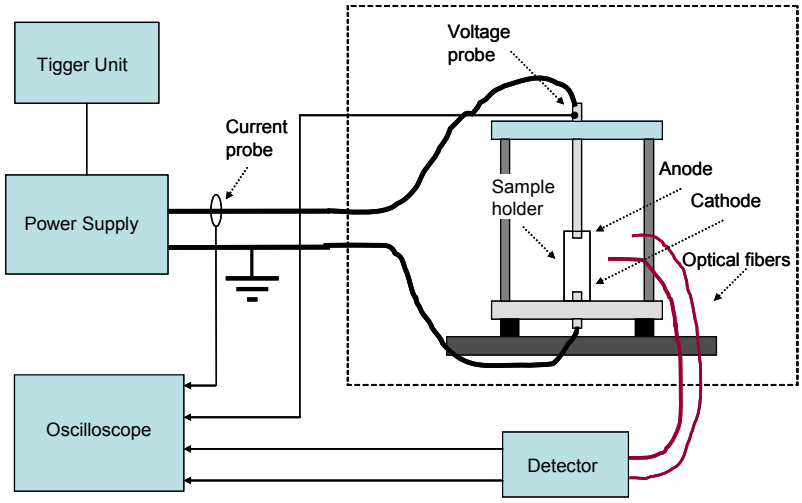

Figure 11. *Schematic picture of the experiment arrangement.*

A tube made of PMMA (Plexiglas), with the dimension (inner diameter x height) Ø4 x 30 mm, Ø9 x 30 mm, Ø9 x 40 mm or Ø10 x 30 mm, was used as sample holder. The sample holder was glued to the bottom plate, made out of stainless steel, over the cathode. The anode, fixed to the top plate made of plastic, was placed so the half-spherical portion of it was in contact with the liquid propellant in the sample holder. An open gap existed between the tube and the anode. The anode and cathode were made out of stainless steel, with a diameter of 8 mm, or of aluminium, with a diameter of 2.2 mm. Figure 12 shows a photograph of the arrangement with a Ø9 x 30 mm sample holder and 8 mm anode and cathode. The height of the arrangement is approx. 150 mm and diameter approx. 120 mm.

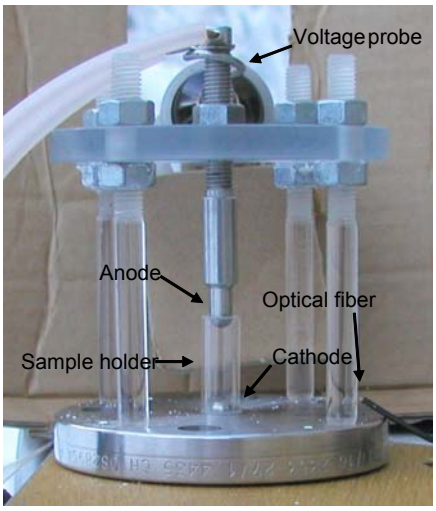

Figure 12. *Photograph of the experiment arrangement.*

4.2 Pulsed-power supply

The pulsed-power supply (PPS) used was not designed for this type of experiments but proved to be useful. The PPS consisted of a 67 μF capacitor bank with a nominal voltage of 30 kV, which at full voltage can store 30 kJ. It was originally designed to power inductive loads, but works well with more or less resistive loads [20]. The system was monitored by remote control, from which charging, dumping and triggering was performed. In the ignition experiments presented here, the charging was limited to 6 kV, corresponding to 1.2 kJ. Evidently, the pulsed power supply is much larger than necessary and could have been much smaller than was the case. A photograph of the pulsed-power supply is shown in Figure 13.

Figure 13. *Photograph of the pulsed-power supply used in the experiments.*

To obtain the impedance characteristics of the system, the pulsed-power supply was discharged into a low resistance (70 mΩ). The system was charged to 6 kV in a series of experiments where the voltage was measured at different locations in the system. Figure 14 shows the measured voltage and current in these experiments. In the left figure, the blue trace is the voltage measured over the capacitors of the pulsed-power supply, the red trace at the output terminal of the pulsed-power supply to which cables are connected and the green trace was measured at the load.

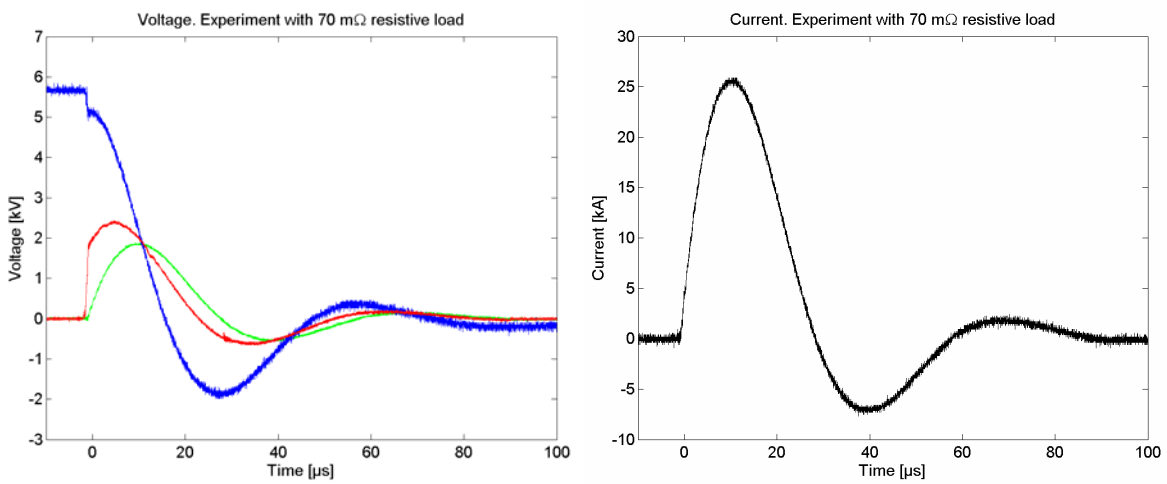

Figure 14. *Voltage (left) and current (right) measurements when using 70 mΩ resistive load.*

By using a simple equivalent electric circuit model, it was possible to obtain the inductance of the different parts of the system. Figure 15 shows the simulations of the system shown in Figure 16. The coloured arrows points out the position of the voltage probe and thus it was possible to identify the distributed inductance and resistances in the pulsed power system.

- 0.1 µH is the internal inductance of the capacitors.
- 0.6 µH and 30 mΩ located in the switch and connecting cables between the capacitors and the output terminal of the pulsed-power supply.
- 0.4 µH is located in the cables to the load.

The distributed capacitance in the system was neglected since it was small compared to the capacitance of the capacitor bank.

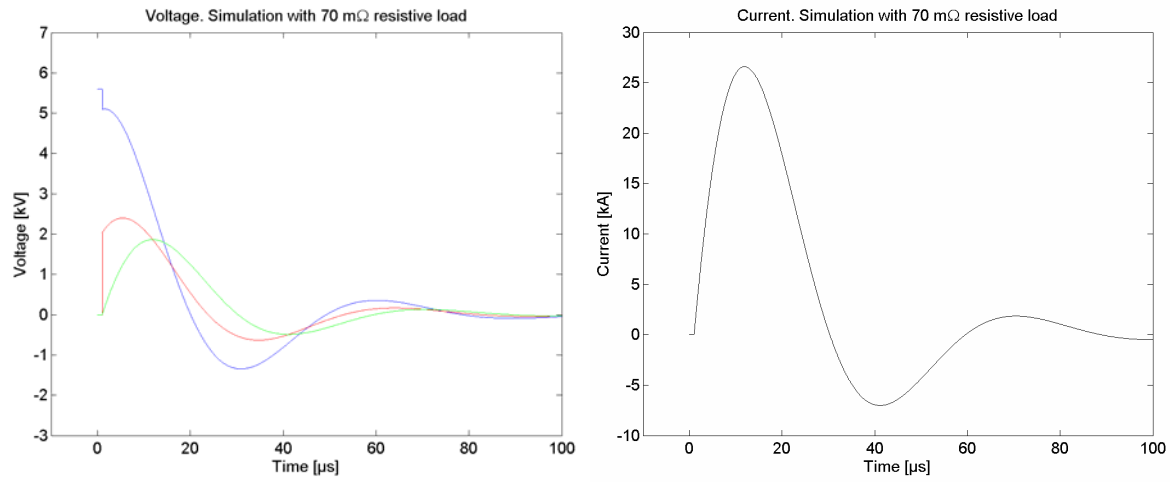

Figure 15. *Simulated voltage (left) and current (right) using the equivalent circuit shown in Figure 16.*

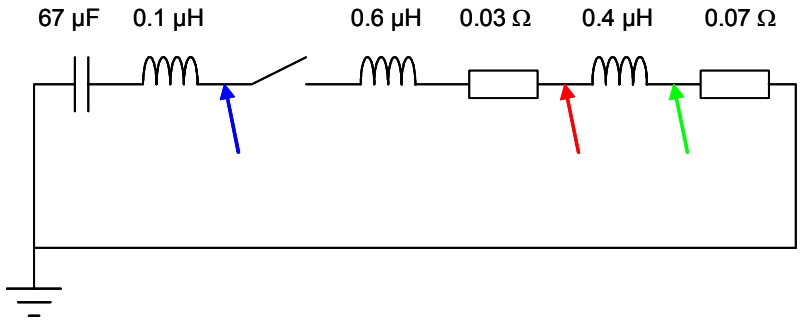

Figure 16. *Equivalent circuit of the pulsed-power supply cables and loads.*

By using the equivalent electric circuit of Figure 16, one can study the influence of loads with higher resistance. Figure 17 shows the discharge current through a 1 Ω and 5 Ω load respectively. The effect of the circuit inductance is that the rise time of the current pulse is decreased. Note that the time scale of influence shown in Figure 17 is shorter than 10 µs. Since the preparatory analysis indicate that the resistance of a typical sample drops from several tens of ohms to several ohms in a time scale of one millisecond (cf. Figure 7), the influence of the circuit inductance can be neglected.

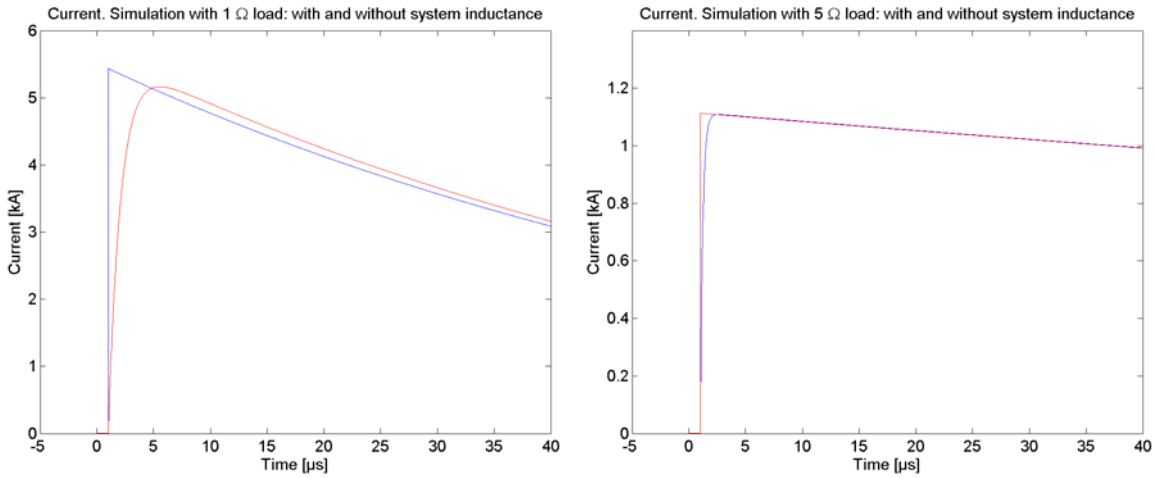

Figure 17. *Simulation of a 1 Ω (left) and 5 Ω (right) load with and without the system inductance.*

4.3 Diagnostics

In order to monitor the system during the experiment, the diagnostics below were used.

4.3.1 Current

The current was measured using a self integrating current probe: Pearson 1423 with a sensitivity of 0.5 V per kA when terminated into 50 Ω or 1 V per kA when terminated into 1 MΩ. Depending on current level attenuators may be used to lower the signal into the oscilloscope, which has a limitation of 1 V/division with 50 Ω termination.

4.3.2 Voltage

The voltage was measured using a Tektronix P6015A with a sensitivity of 1 V per kV. The probe is terminated with 1 MΩ at the oscilloscope. The voltage probe has a voltage limit of 20 kV DC, or 40 kV pulsed voltage.

4.3.3 Opto detectors

Standard nylon optical fibers was pointed at the propellant sample of the experiment, and connected via opto detectors to the oscilloscope at 1 MΩ.

4.3.4 High-speed video camera

In some of the experiments, a Photron APX high-speed video camera was used. The cameras was set to the frame rate 10000 frames per second with resolution 512 x 256 pixels or a frame rate 20000 frames per second with resolution 128 x 256 pixels.

4.3.5 Oscilloscope

LeCroy oscilloscopes of different versions were used with sampling rate and analogue bandwidths of at least 500 MS/s and 1 GHz respectively. This was more than sufficient considering that the frequency content of the discharge pulse was 16 kHz in the experiments using the 70 mΩ load. In some cases, an insulating transformer was used between the oscilloscope and the power grid.

5 Experimental Results and Analysis

The complete experiment matrix is presented in the Appendix, together with a full documentation of all experimental results for all experiments where ignition was obtained.

5.1 Typical Experiment Results

Figures 18 and 19 shows typical results from one experiment, in this case experiment 041126-005, where the pulsed-power generator was charged to 4 kV, the propellant was FLP-105, the dimension of the sample holder was Ø9x30 mm and the distance between the anode tip and the cathode tip was 25 mm.

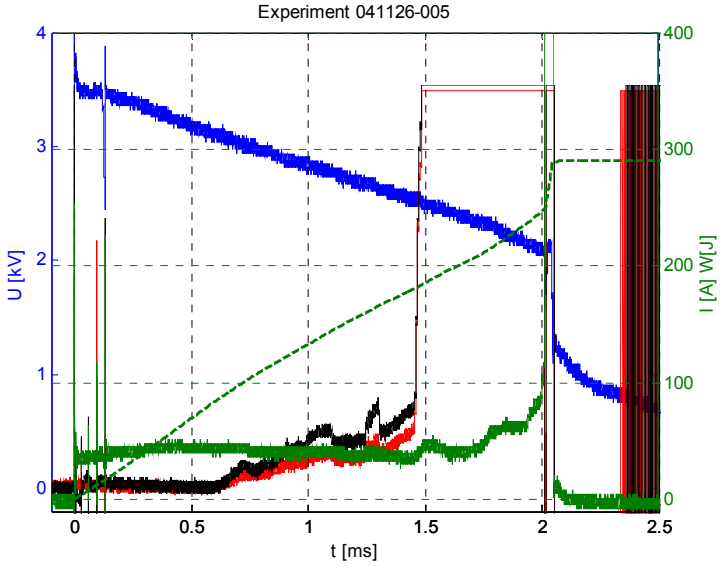

Figure 18. *The voltage across (blue) and the current through (solid green) the sample together with deposited electric energy (dashed green) and opto 1 and opto 2 signals (red and black).*

Figure 18 shows the voltage, current, opto signals and the derived dissipated energy, (integration of voltage times current). The optical signal at about 0.6 ms indicate the initial ignition of the propellant, whereas the steep rise and saturation of the optical signal at 1.5 ms indicate the full ignition of the propellant sample. The dissipated energy for the initial ignition was about 100 J and for the full ignition 180 J. The pulsed power supply continues to deliver current through the electrical conducting plasma, i.e. the burning propellant. Figure 19 shows the current and the derived resistance (voltage divided by the current).

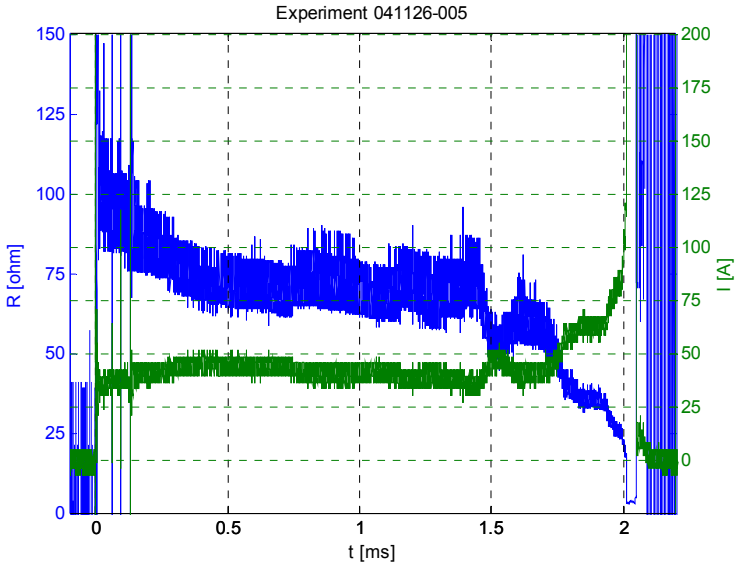

Figure 19. *The current through the sample (green) together with the sample resistance (blue).*

5.2 Varied parameters

The experiments were performed with two different propellants, FLP-105(xxx) and FLP-106(xxx) where xxx is the batch number. The FLP-106 has a higher conductivity than the FLP-105. Voltage levels of 4 kV and 4.7 kV have been used resulting in successful ignition of both propellants. Ignition has also been achieved with 2.7 kV for the smallest sample size (see Table 7).

The sample holders used had the dimensions Ø4 x 30 mm, Ø9 x 30 mm, Ø9 x 40 mm or Ø10 x 30 mm. With sample holders with a diameter of 9 and 10 mm, the diameter of the hemispherical anode and cathode used was 8 mm, and with the sample holder with diameter Ø4 mm, Ø2.2 mm anode and cathode was used. Table 7 gives the total volume of the propellant sample.

Table 7. Sample holders and volumes.

Sample holder Ø: inner diam x: height [mm]	**Anode and cathode diameter [mm]**	**Anode-cathode gap [mm]**	**Volume of propellant [cm^3]**
Ø4x30	2.2	27	0.37
Ø9x30	8	25	1.84
Ø9x40	8	25	2.48
Ø10x30	8	30	2.29

5.3 Result from the high-speed video

Three of the experiments were recorder with a high-speed camera with the frame rate 10000 frames per second or 20000 frames per second. The aperture setting for the high-speed video camera optics was differently adjusted for the three shots.

Figure 20 shows the high-speed camera pictures from experiment 041207-001. The frame rate was 10000 frames per second and the exposure time for each frame was 100 µs.

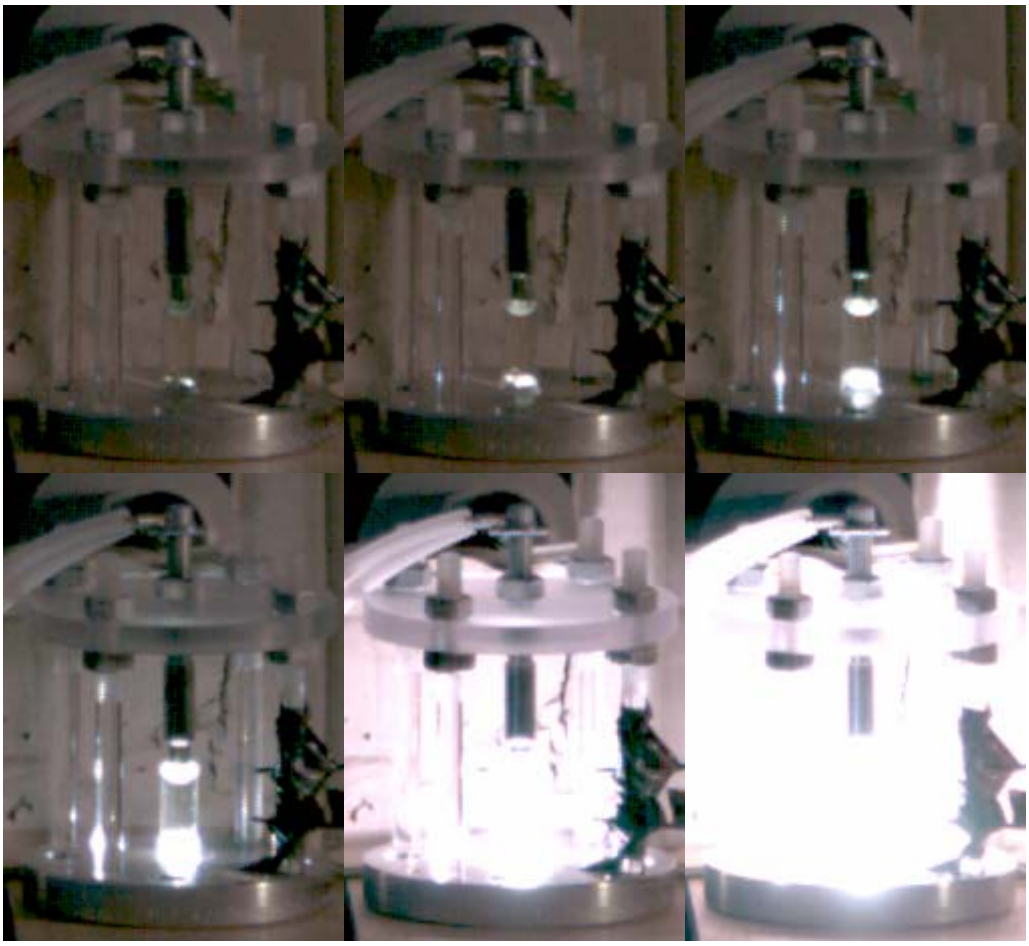

Figure 20. *High- speed video pictures from experiment 041207-001, frame rate 10000 fps.*

Figure 21 shows the high-speed video pictures from experiment 041207-002. The frame rate was 20000 frames per second and the exposure time for each frame was 50 μs.

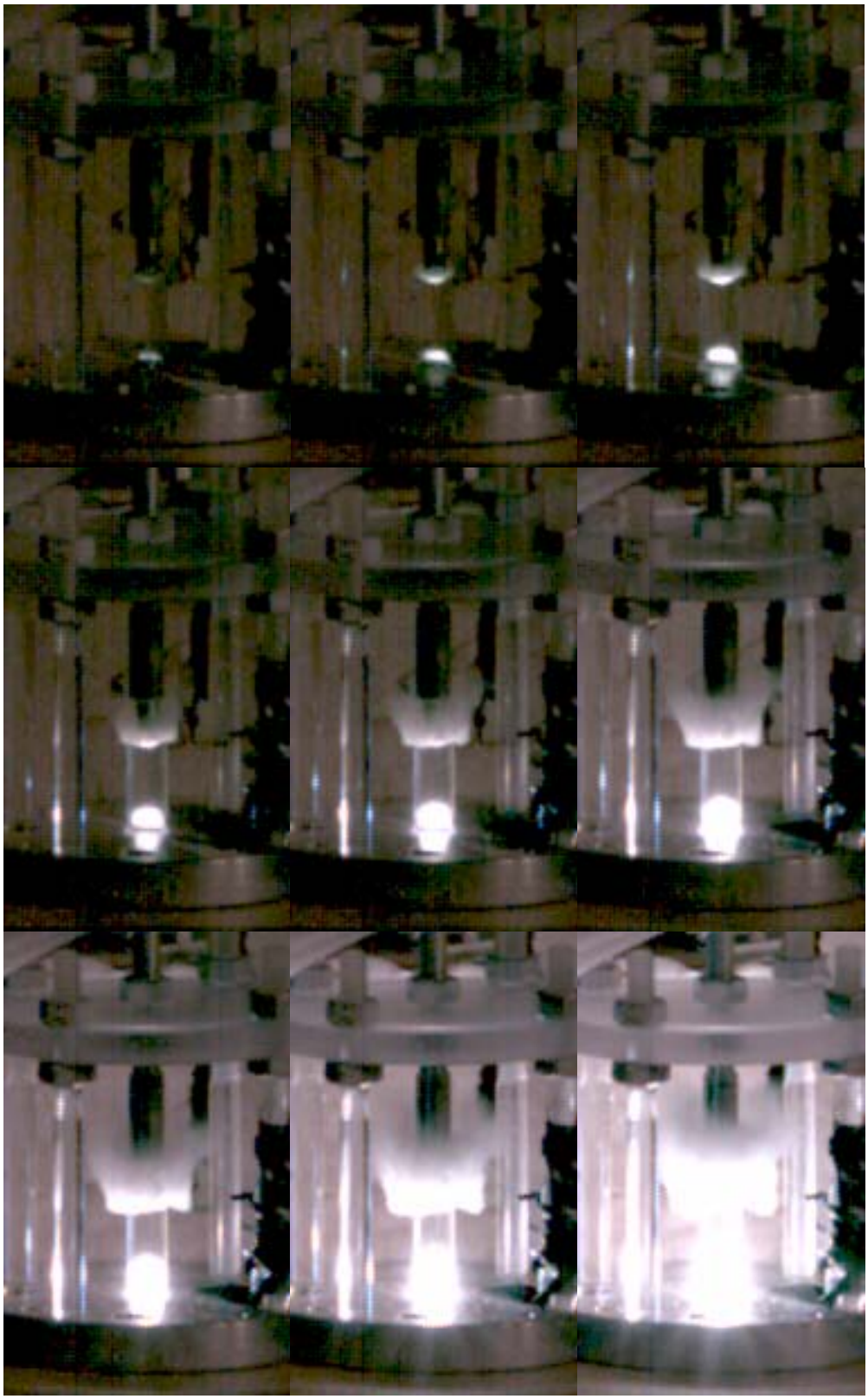

Figure 21. *High-speed video pictures from experiment 041207-002, frame rate 20000 fps.*

Figure 22 shows the high-speed video pictures from experiment 041207-003. The frame rate was 20000 frames per second and the exposure time for each frame was 50 μs.

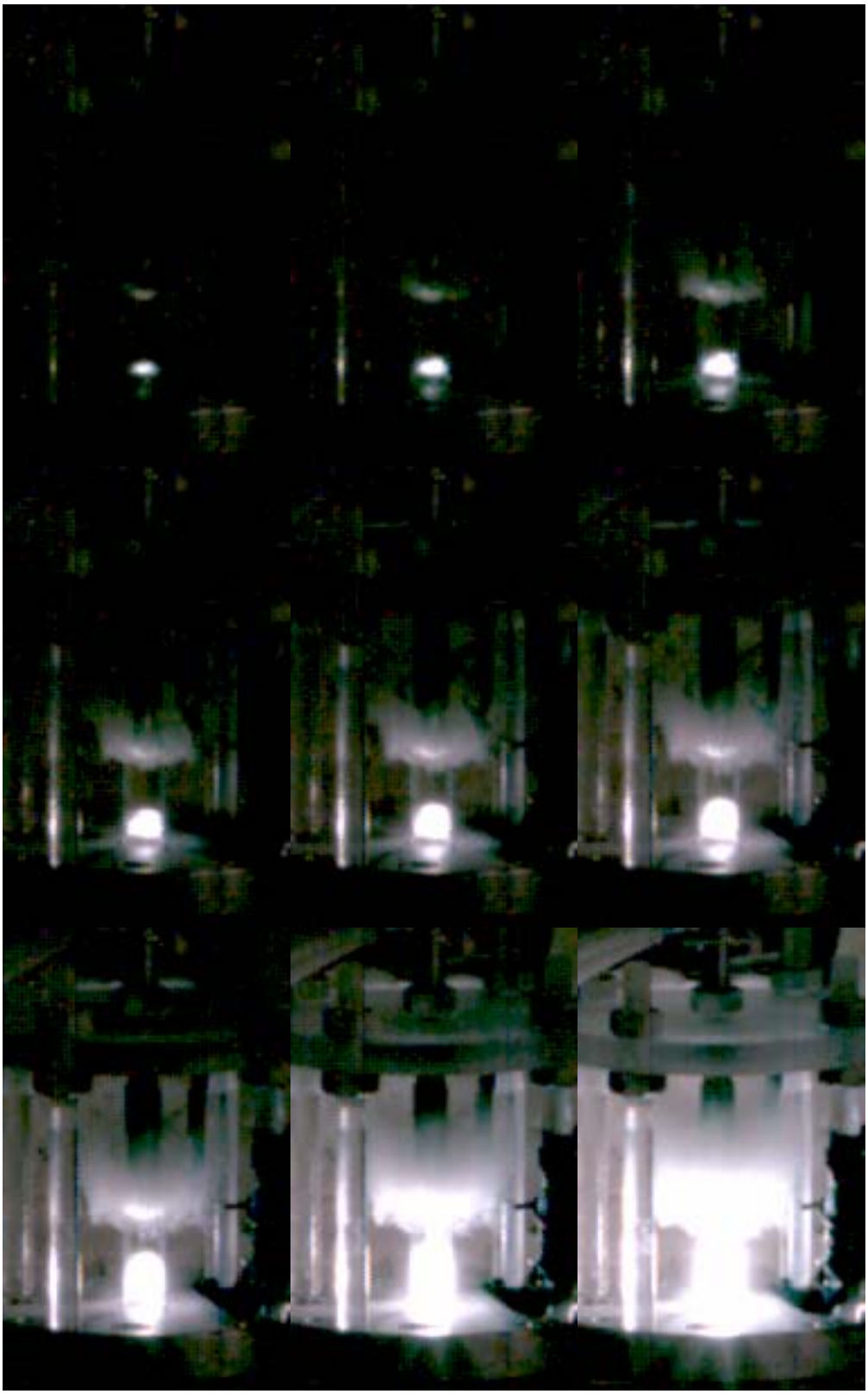

Figure 22. *High-speed video pictures from experiment 041207-003, frame rate 20000 fps.*

6 Discussion

It was expected that the propellant would be heated uniformly until it reached the thermal ignition temperature. Due to heat losses to the surrounding, the highest temperature would be found in the middle of the sample, and it was thus expected that the ignition would be initiated in the very centre of the propellant. Thus, the electric energy needed to obtain ignition would approximately be equal to the energy needed to raise the bulk temperature to the ignition temperature. However, the result shows that the ignition was initiated close, or on the surface, of the electrodes, and the electric energy required was only a fraction of what was expected. Apparently, some local phenomena at the electrodes are responsible for the ignition. This might be due to:

- Non-uniform heating resulting in higher temperatures at the electrodes
- Catalytic influence from the metal electrodes
- Electrochemical reactions at the electrodes

Non-uniform heating is not likely, due to the design of the electrode configuration. However, since the electrodes were not polished between each experiment, micro protrusions might have caused hotspots of the electric fields. To determine if the ignition is due to catalytic or electrochemical reactions, further research is needed.

The sequence of the events is interpreted in the following way, where mainly the typical result presented in Figures 18 and 19 are used together with the high-speed video recordings. The sample is heated by the current forced through it. The light signal from the optical fibres indicates that the propellant is ignited. It is not possible to identify the ignition in the voltage and current signals. From the high-speed video recordings, one can see that the initial ignition first starts at the lower electrode (the cathode), followed by ignition at the anode. The ignition front travels from the cathode towards the anode. Since the sample holder is open at the anode, the internal pressure forces the propellant out of the sample holder at the anode, thus creating a burning plume. After a certain time, the ignition front reaches the anode and a full ignition occurs, saturating the optical fibre measurements. This full ignition is not possible to identify in the voltage measurements, and can barely be detected in the current measurements. Finally, a steep current increase and a sudden drop in voltage are observed, indicating that an arc discharge has short-circuited the electrode gap. Such a breakdown is not observed in all cases.

Numerical simulations, using the model presented in Section 3, are performed for the typical case shown in Figures 18 and 19. The results of the simulation are shown in Figure 23. The early values of the voltage, current and resistance are well reproduced by the model, but later the results deviate. The temperature predicted by the model is far below any ignition temperature and ignition occurs earlier than predicted, as seen by the optical signal in Figure 18. The model assumes that the heating of the sample is uniform and the bulk temperature is calculated. As seen in the high-speed video pictures, the ignition is not uniform but starts at the electrodes.

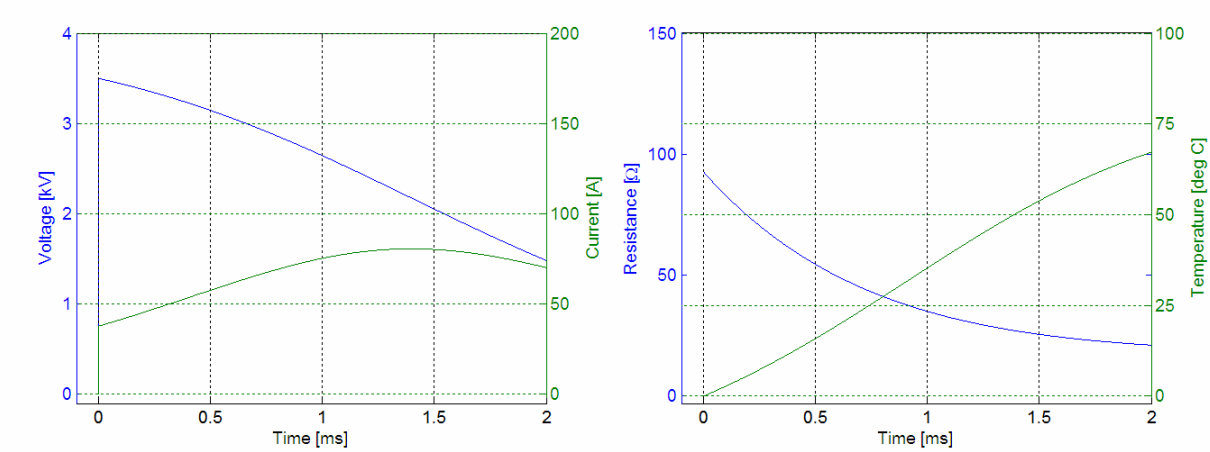

Figure 23. *Simulation of the case shown in Figures 18 and 19.*

Igniting the propellant by resistive heating requires the lowest amount of electrical energy, as discussed in the introduction. However, not only should the electric energy needed be minimized, but the weight of any supplementary devise must also be as low as possible. In the case of resistive heating, a pulsed-power supply including a storage capacitor is required. The size and weight of the capacitor will be determined by the minimum energy needed, which in turn is determined by the minimum amount of propellant that must be heated to obtain sustained combustion. For the larger sample size, about 100 J was required to ignite the sample, which is several times lower than if assuming uniform heating of the sample. The conclusion is that some electrode effects play a decisive role in the ignition. In the literature [21] a capacitor with the following performance was found: 2 MJ/m^3, 1.7 kJ/kg. Scaling this to 100 J shows that a capacitor for this application will have a volume of 0.05 dm^3 and a weight of 0.06 kg. The amount of propellant used in our first experiments was approximately 2.5-3 g. Later this was decreased to 0.5 g by using a smaller sample holder. When using the smaller sample holder, the ignition was initiated in the range of 10 to 20 J and full ignition was obtained at approximately 50 J. This would require a capacitor weighting some tens (10-30 g) of grams. The complete pulsed-power supply is estimated to weight of the order of one kilogramme and occupies a volume of the order of one cubic decimetre, if getting the electric energy from the on-board electric power unit. If a vehicle requires a total impulse equivalent to 100 kg of hydrazine, this would require only 88 kg of FLP-105. Hence, the supplementary weight of the pulsed-power supply can be compensated for, due to the higher specific impulse of the FLPs. One capacitor can also be used for several rocket engines. For an optimal use of energy, it would be interesting to know if the initial ignition continues to full ignition if the current is switched off after the initial ignition.

In a rocket engine, the propellant is injected into the combustion chamber at a desired flow rate. When the propellant enters the combustion chamber, it is important to obtain rapid ignition. A too slow ignition will lead to accumulation of unburned propellant. When ignition occurs this might lead to pressure spikes, or failure of the combustion chamber. It is not unusual for bipropellants that the ignition delay is in the order of 10 ms. The results from these experiments have shown that full ignition can be obtained within 2 ms. It thus seems that the ignition delay would not be a matter of major concern.

The smaller amount of propellant that is electrically heated, the less electric energy is needed. If the initial amount of propellant is too small, ignition might be impossible due to heat loss to the surrounding. Once the propellant has ignited in the combustion chamber, a large amount

of chemical energy is released. If the initial amount of propellant ignited is large enough, it will in turn ignite the following propellant entering the combustion chamber, and thus sustained combustion will be achieved. The minimum amount of propellant that must be electrically ignited to achieve sustained combustion must be determined experimentally.

Intuitionally it seems that a larger rocket engine would require a larger amount of electric energy to ignite. However, this is not necessarily the case, since, by proper design, a small engine can be used as an igniter torch. A very large engine, however, might need several igniter torches to obtain rapid flame spreading, but within reasonable changes in size, the electrical energy needed might be independent of engine size. The capacitor can be recharged from the internal electrical system of the vehicle, and the charging time will depend on how much power is available.

7 Conclusions

ADN-based liquid propellants have been successfully ignited by resistive heating. The required energy was substantially less than expected, thus giving great potential for minimizing the power supply. The ignition was not due to uniform heating of the sample, as expected. Instead, the ignition seemed to be locally initiated at the electrodes. Very fast ignition, less than < 2 ms, was obtained. A pulsed-power supply for this application is expected to have a weight of the order of one kilogram. The fast ignition and the expected low weight of the capacitor show that this type of ignition method can be used in a flying vehicle as a missile or a spacecraft.

8 Future work

Future work should be focused on studying the ignition process in more detail, in particular the influence of the electrodes, with a smaller pulsed-power supply. To decrease the energy needed and the weight of the pulsed-power supply, it would be interesting to further decrease the size of the ignition device, and to study if the initial ignition will propagate to full ignition after cutting off the voltage, after initial ignition have been obtained. How to integrate this type of ignition device in micro-pulse rocket thrusters and larger rocket engines should also be investigated.

Acknowledgements

The authors would like to thank Sten Andreasson and Mose Akyuz for valuable discussions and Kaj Ormegard for assistance with the high-speed video camera.

References

1. B. Palaszewski, L. S. Ianovski, P. Carrick, Propellant Technologies: Far-Reaching Benefits for Aeronautical and Space-Vehicle Propulsion, *Journal of Propulsion and Power* **1998**, *14*, 641-648.
2. V. Bombelli, D. Simon, T. Marée, Economic Benefits of the use of Non-Toxic Monopropellants for Spacecraft Applications, AIAA 2003-4783, *39th AIAA/ASME/SAE/ASEE Joint Propulsion Conference*, 20-23 July, Huntsville, AL, USA **2003**.
3. D. M. Zube, E. J. Wucherer, B. Reed, Evaluation of HAN-Based Propellant Blends, AIAA 2003-4643, *39th AIAA/ASME/SAE/ASEE Joint Propulsion Conference*, 20-23 July, Huntsville, AL, USA **2003**.
4. A. G. Accettura, L. De Rose, J. Gonzalez del Amo, Advanced Propulsion System Scenario in the frame of Propulsion 2000 Program, *Tenth International Workshop on IN-SPACE PROPULSION*, September 21-25, Lerici, La Spezia, Italy **2003**.
5. B. D. Reed, On-Board Chemical Propulsion Technology, *10th International Workshop on Combustion and Propulsion*, 21-25 September, Lerici, La Spezia, Italy **2003**.
6. M. Ford, *European Space Technology Harmonisation Technical Dossier on Mapping: Chemical Propulsion - Green Propellants*, Report TOS-MPC/2167/MF, **2002**, ESA/ESTEC.
7. E. J. Wucherer, S. Christofferson, Assessment of High Performance HAN-Monopropellants, AIAA 2000-3872, *36th AIAA/ASME/SAE/ASEE Joint Propulsion Conference*, 16-19 July, Huntsville, AL, USA **2000**.
8. N. Wingborg, R. Tryman, ADN-Based Monopropellants for Spacecraft Propulsion, *10th International Workshop on Combustion and Propulsion*, 21-25 September, Lerici, La Spezia, Italy **2003**.
9. N. Wingborg, C. Eldsäter, H. Skifs, Formulation and Characterization of ADN-Based Liquid Monopropellants, *2nd International Conference on Green Propellants for Space Propulsion*, 7-8 June, Chia Laguna, Sardinia, Italy **2004**.
10. K. Anflo, T. A. Grönland , N. Wingborg, Development and Testing of ADN-Based Monopropellants in Small Rocket Engines, AIAA 2000-3162, *36th AIAA/ASME/SAE/ASEE Joint Propulsion Conference*, 16-19 July, Huntsville, AL, USA **2000**.
11. A. G. M. Marée, J. L. P. A. Moerel, W. H. M. Welland-Veltmans, F. J. M. Wierkx, J. Zevenbergen, Technology Status of HNF-Based Monopropellants for Satellite Propulsion, *2nd International Conference on Green Propellants for Space Propulsion*, 7-8 June, Chia Laguna, Sardinia, Italy **2004**.
12. M. Fick, P. Schiebener, J. L. P. A. Moerel, R. P. v. d. Berg, H. M. Sanders, W. H. M. Welland-Veltmans, Industrial Benefits of Applying HNF in Monopropellant Satellite Propulsion, *First International Conference on Green Propellants for Space Propulsion*, 20-22 June, Noordwijk, The Netherlands **2001**.
13. H. F. R. Schöyer, W. H. M. Welland-Veltmans, J. Louwers, P. A. O. G. Korting, A. E. D. M. v. d. Heijden, H. L. J. Keizers, R. P. v. d. Berg, Overview of the Development of Hydrazinium Nitroformate-Based Propellants, *Journal of Propulsion and Power* **2002**, *18*, 138-145.
14. C. Kappenstein, N. Pillet, A. Melchior, New Nitrogen-Based Monopropellants (HAN, ADN, HNF, ...). Physical Chemistry of Concentrated Ionic Aqueous Solutions, *Propulsion for Space Transportation of the XXIst Century*, 13-17 May, Versailles, France **2002**.

15. N. Wingborg, *ADN based liquid monopropellants*, Report FOA-RH--99-00430-310--SE, **1999**, Försvarets Forskningsinstitut, FOA.
16. N. Wingborg, *Flytande drivämnen till smarta vapen*, Report FOI-RH--0209--SE, **2003**, Totalförsvarets Forskningsinstitut, FOI.
17. H. Östmark, U. Bemm, A. Langlet, R. Sandén, N. Wingborg, The Properties of Ammonium Dinitramide (ADN): Part 1, Basic Properties and Spectroscopic Data, *Journal of Energetic Materials* **2000**, *18*, 123-128.
18. C. D. Brown, *Spacecraft Propulsion*, AIAA Inc., Washington **1995**, p.
19. *CRC Handbook of Chemistry and Physics*, 80th ed., **2000**, p. 8-108.
20. P. Appelgren, G. Bjarnholt, T. Hultman, T. Hurtig, S. E. Nyholm, *High voltage generation and power conditioning wiht TTHPM*, Report FOA-R--00-01760-612--SE, **2000**, FOA Defence Research Establishment.
21. F. Podeyn, H. G. Wisken, T. H. G. G. Weise, High energy density capacitors for pulsed power applications, *Int. Conf. on Pulsed Power Applications*, Gelsenkirchen, Germany **2001**.

Appendix

The complete experiment matrix is presented in this Appendix, together with a full documentation of all experimental results for all experiments where ignition was obtained. The experimental matrix is shown in the table below.

Some tests were performed with a 50 Hz 230 V AC power source connected to the load via a 10-Ω resistor, but the propellant vaporised during the first cycle and no ignition was achieved.

Experiment	Propellant[a]	Sample holder [mm]	Sample mass [g]	Charging voltage [kV]	A-C gap [mm]	A & C diameter [mm]	Propellant temp [°C]	Time to full ignition [ms]	Note[b]
041112-004	FLP106 (771)	∅9×40	3.38	5	30	8	20	n/a	
041119-001	FLP105 (770)	∅9×30	2.60	4	25	8	20	2.4	O1, V
041119-002	FLP105 (765+770)	∅10×30	3.23	5.5	25	8	20	0.45	O1, V
041119-003	FLP105 (771)	∅9×30	2.60	4.7	25	8	20	0.75	O1, V
041126-001	FLP105 (775)	∅9×30	2.62	4	25	8	0	2.0	O1, O2
041126-002	FLP106 (771)	∅9×30	2.54	4	25	8	0	1.0	O1, O2
041126-003	FLP106 (----)	∅9×30	2.54	4	25	8	0	1.1	O1, O2
041126-004	FLP106 (----)	∅9×30	2.54	4.7	25	8	0	0.6	O1, O2
041126-005	FLP105 (771)	∅9×30	2.62	4	25	8	0	1.5	O1, O2
041126-006	FLP105 (775)	∅9×30	2.62	4.7	25	8	0	0.95	O1, O2
041207-001	FLP105 (776)	∅9×30	2.62	4	25	8	0	0.5	HS, O1, O2
041207-002	FLP106 (777)	∅9×30	2.54	4	25	8	0	0.35	HS, O1, O2
041207-003	FLP105 (776)	∅9×30	2.54	4	25	8	0	0.5	HS, O1, O2
041222-001	FLP106 (777)	∅4×30	0.51	4	27	2.2	0	0.3	O1, O2
041222-002	FLP105 (778)	∅4×30	0.53	2.75	27	2.2	0	1.5	O1, O2

a) Batch number in parenthesis
b) O1 – opto fibre aiming at the centre of the sample holder, O2 – opto fibre aiming at the anode tip, V – normal video camera, HS – High speed video camera at 10000 fps (041207-001) or 20000 fps (041207-002 and -003).

In the following diagrams the measured and the calculated data are presented. There are three plots for every experiment.

- The first shows the voltage over the load (blue curve), the current trough the load (solid green curve) and the energy deposited into the load (dashed green curve) and, if present, opto 1 signal, aiming at the centre of the sample holder (red curve) and the opto 2 signal, aiming at the anode (black curve).

- The second shows again the voltage over the load (blue curve) and the power dissipated at the load (green curve).

- The third shows the resistance of the propellant (blue curve) and the current through the load (green curve).

Experiment 041112-004

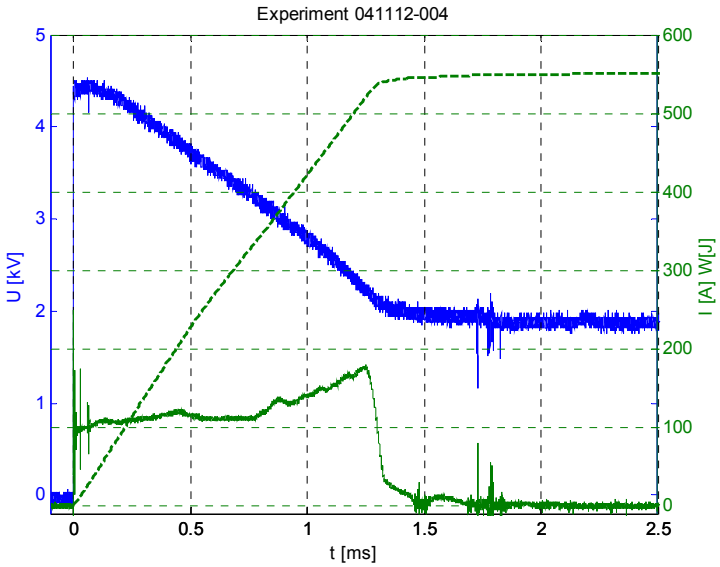

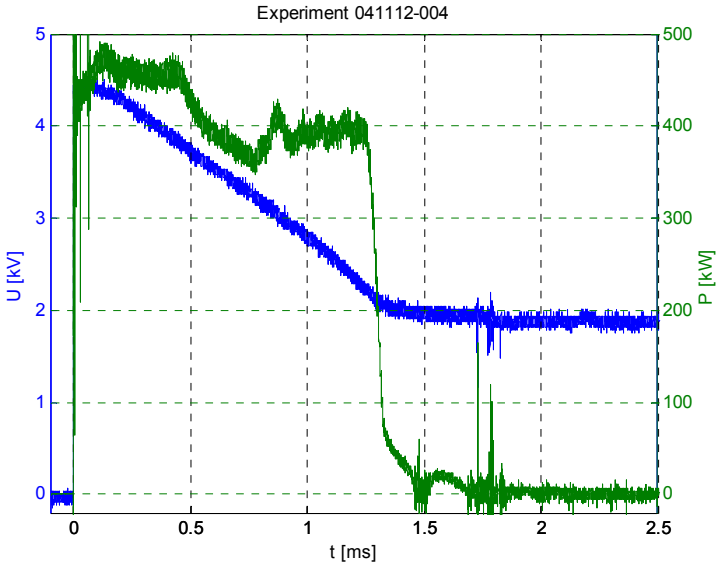

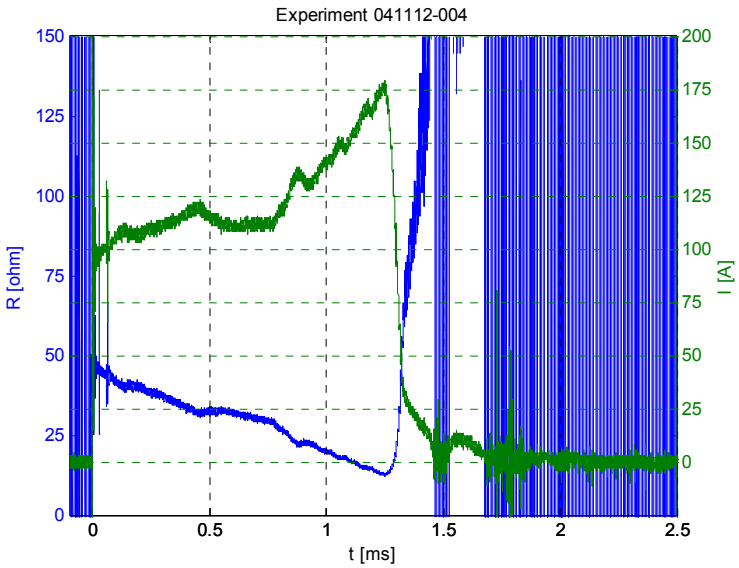

Experiment 041119-001

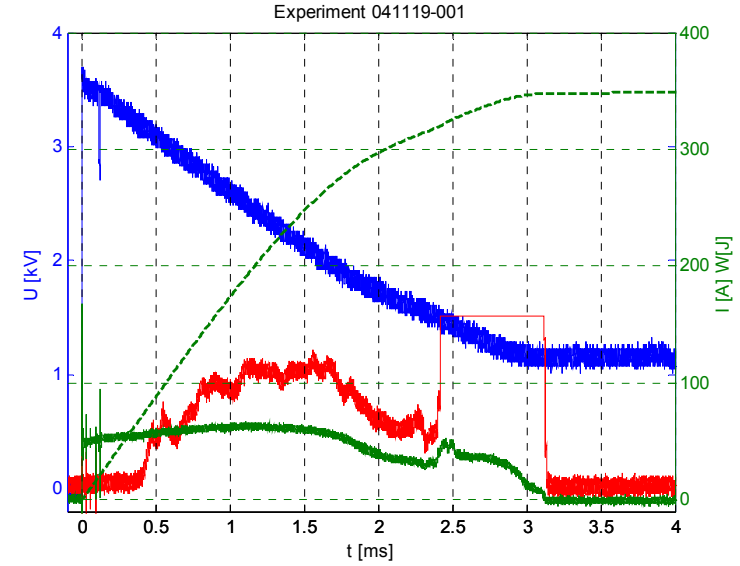

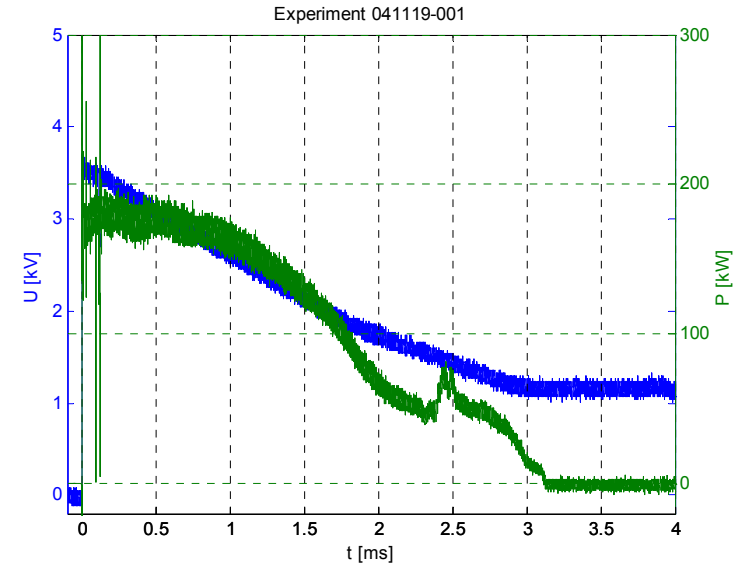

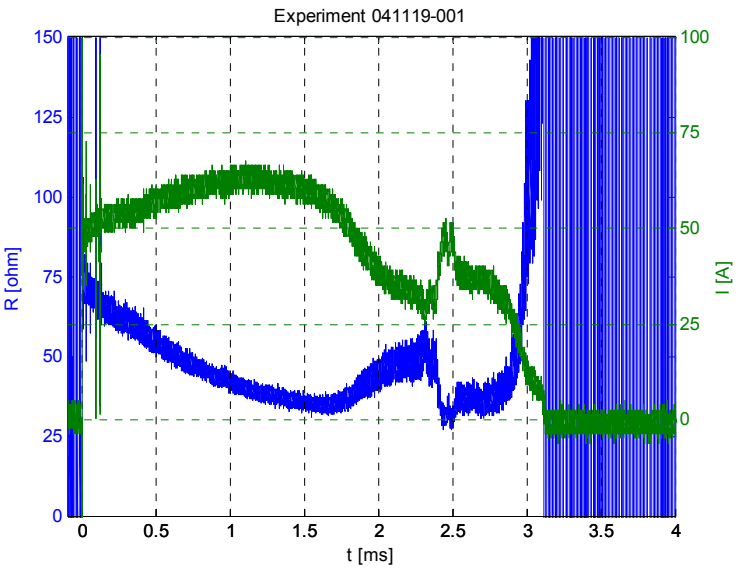

Experiment 041119-002

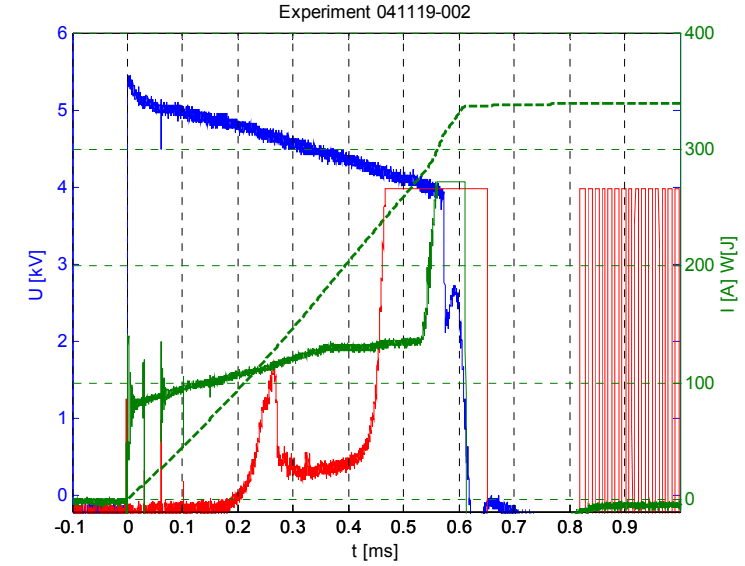

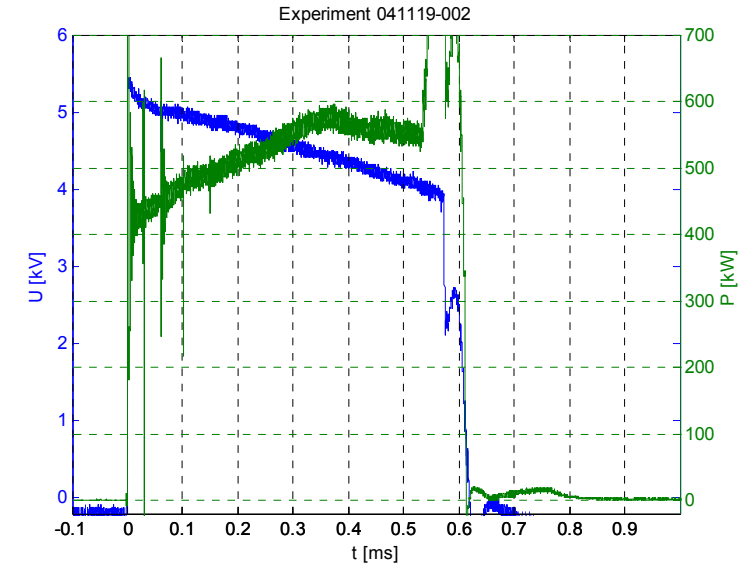

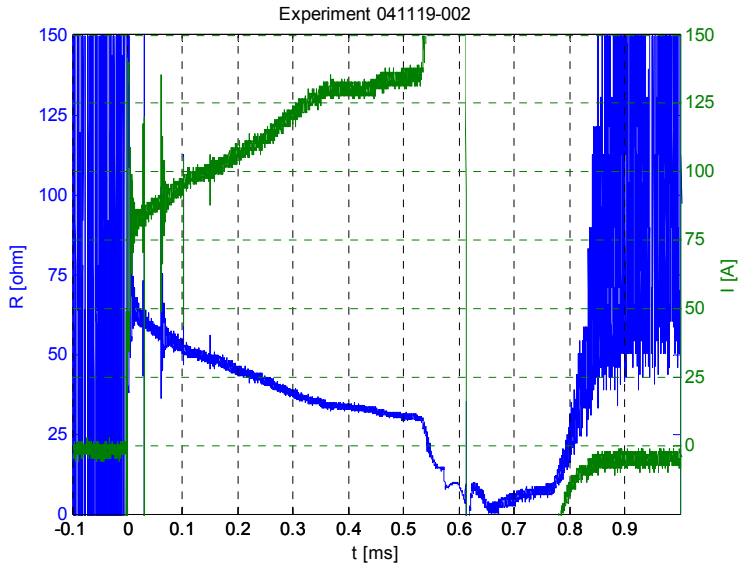

Experiment 041119-003

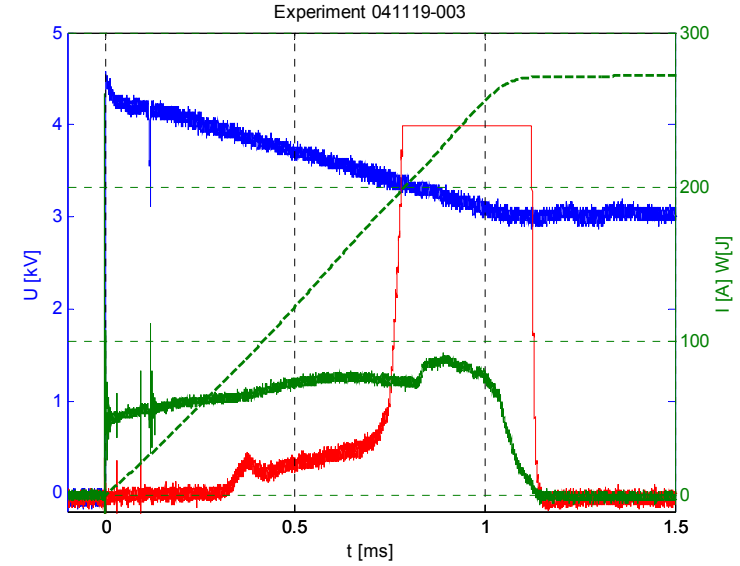

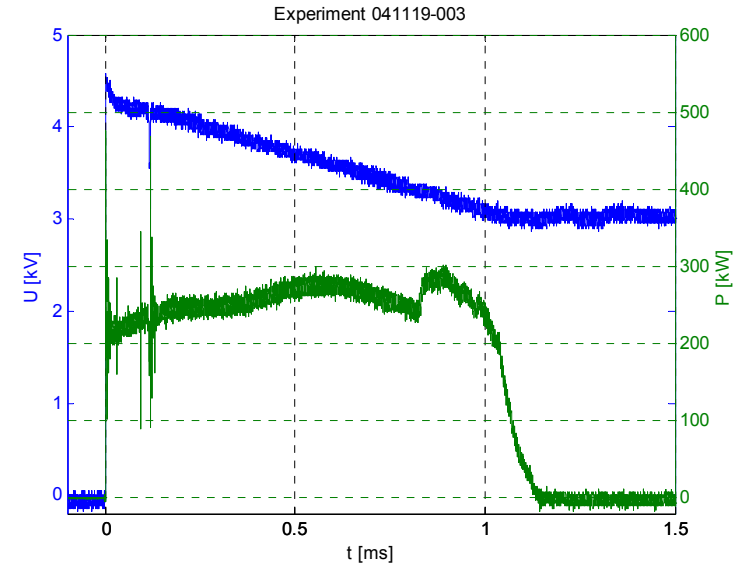

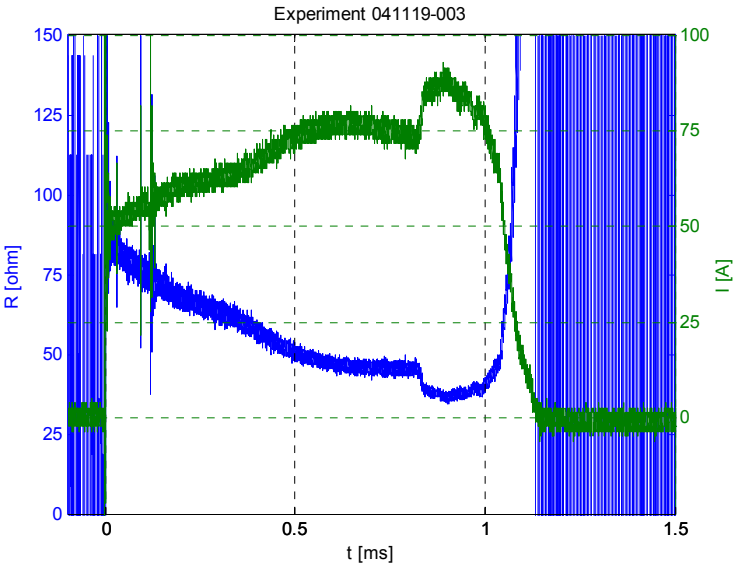

Experiment 041126-001

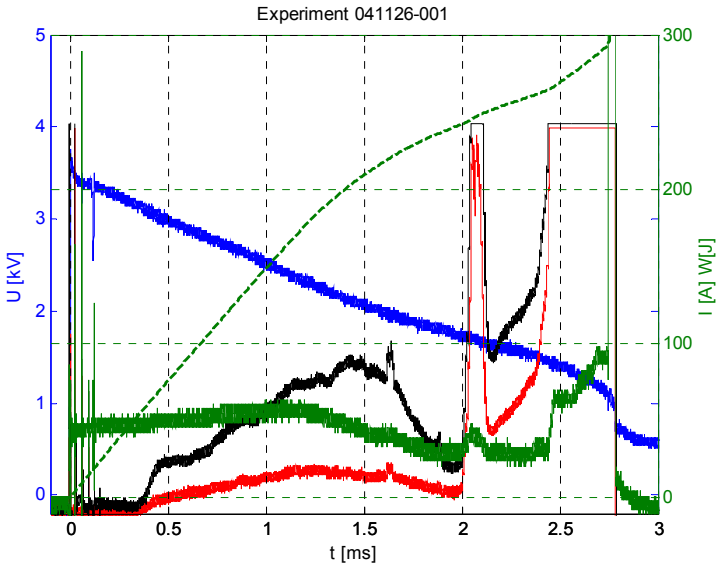

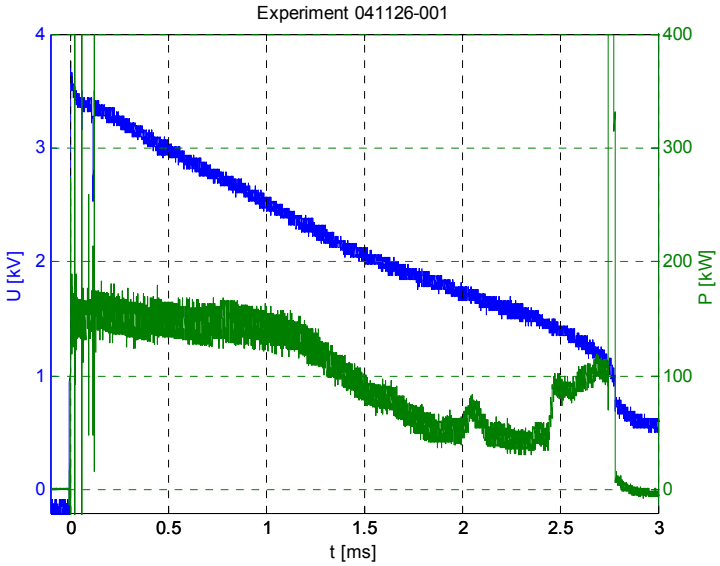

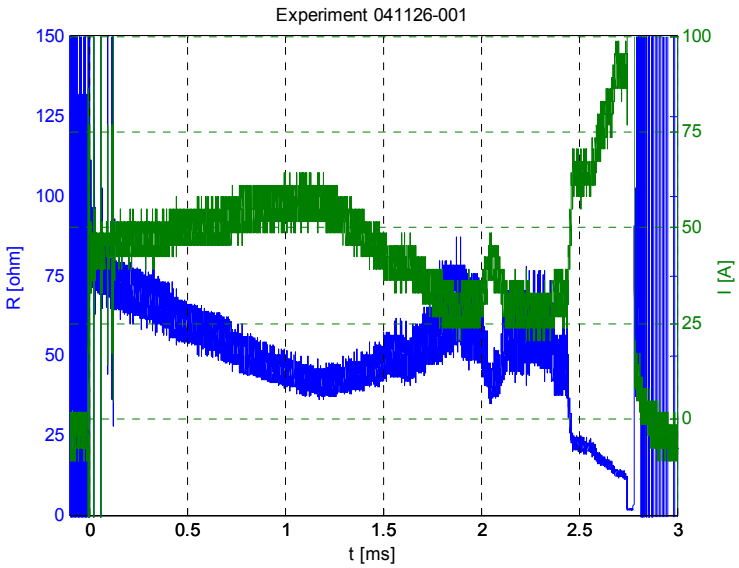

Experiment 041126-002

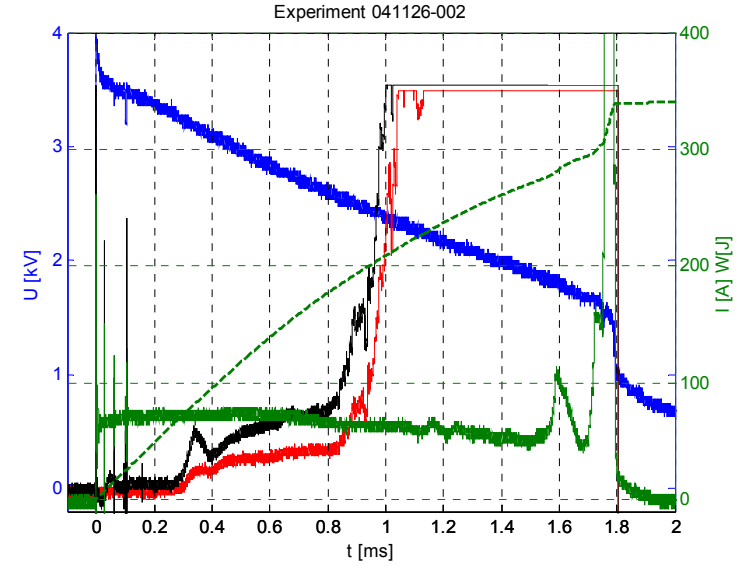

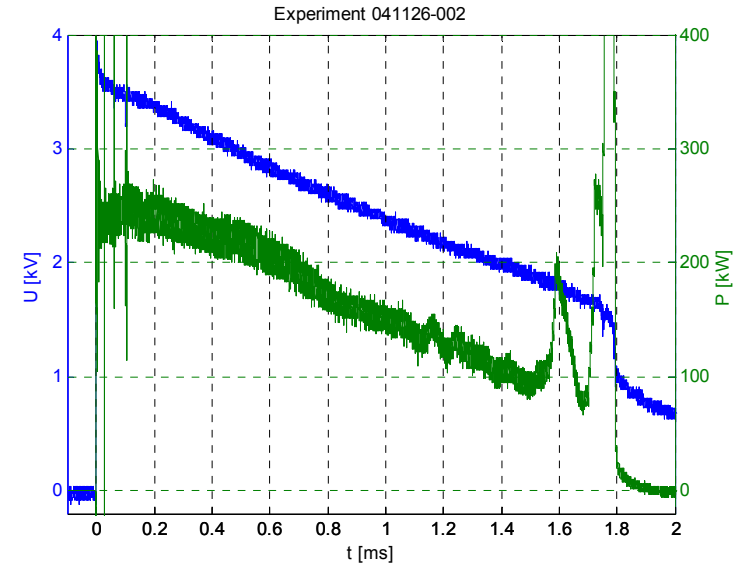

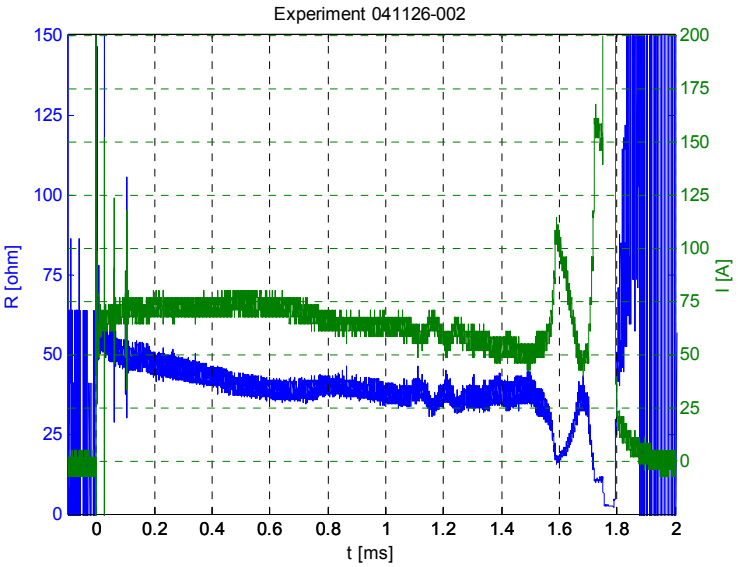

Experiment 041126-003

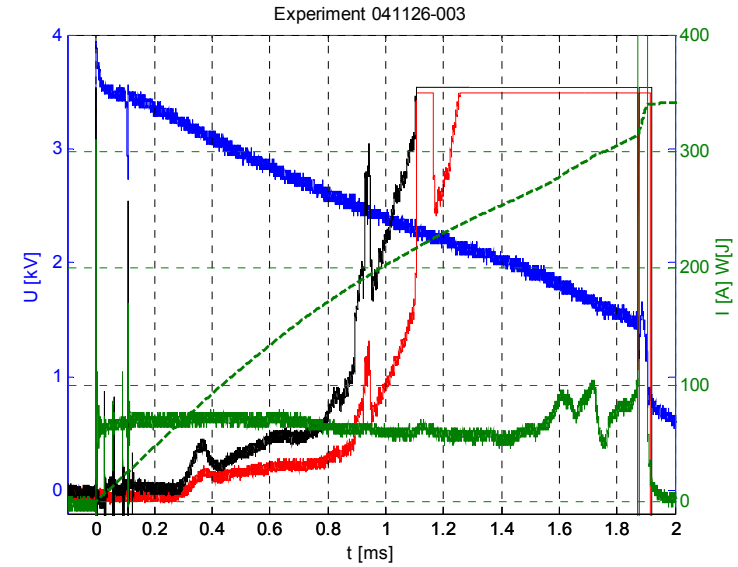

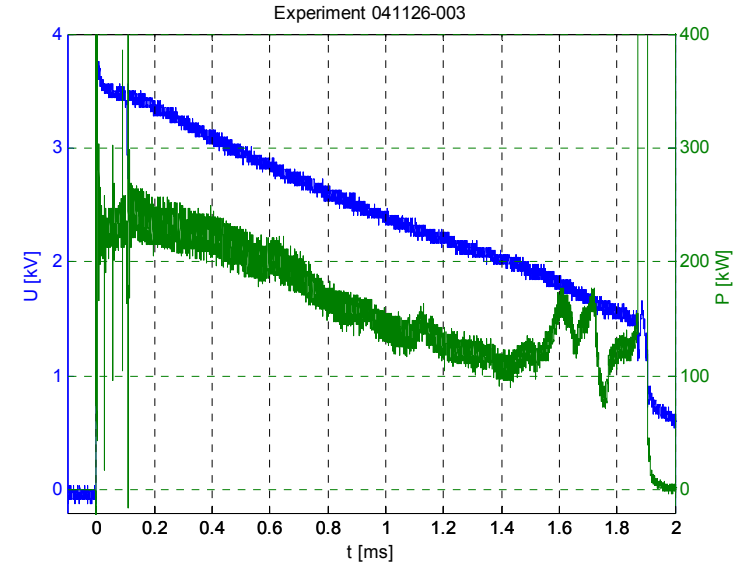

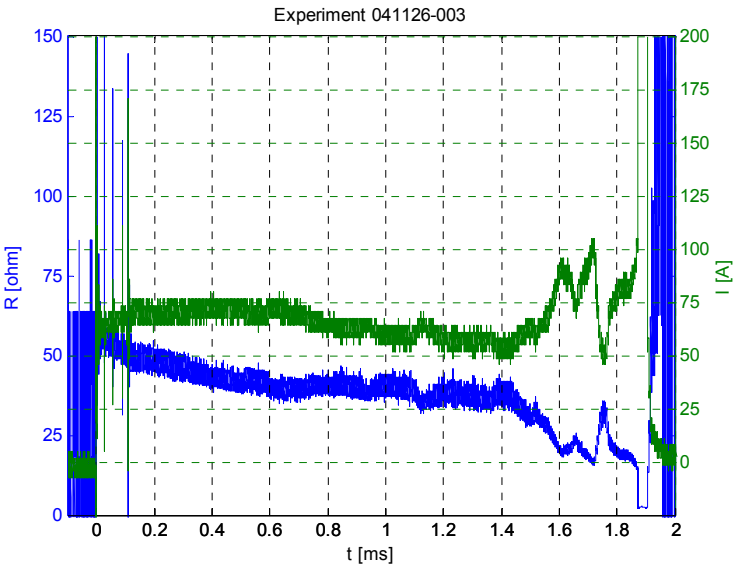

Experiment 041126-004

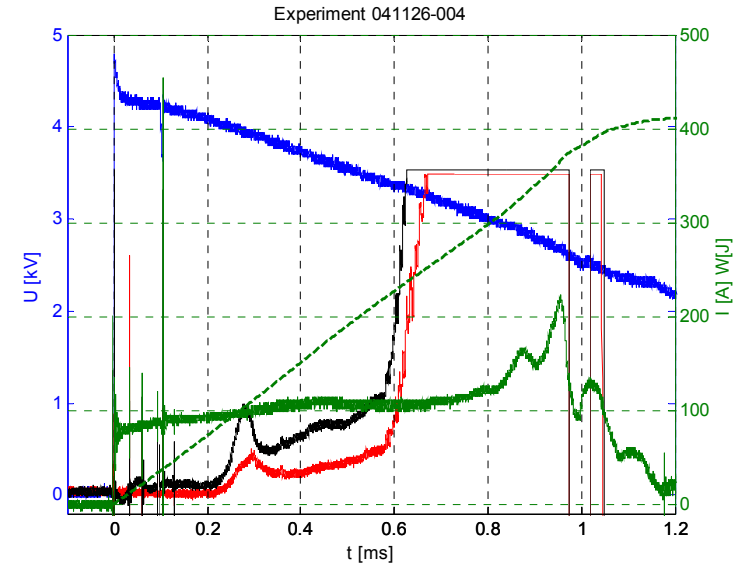

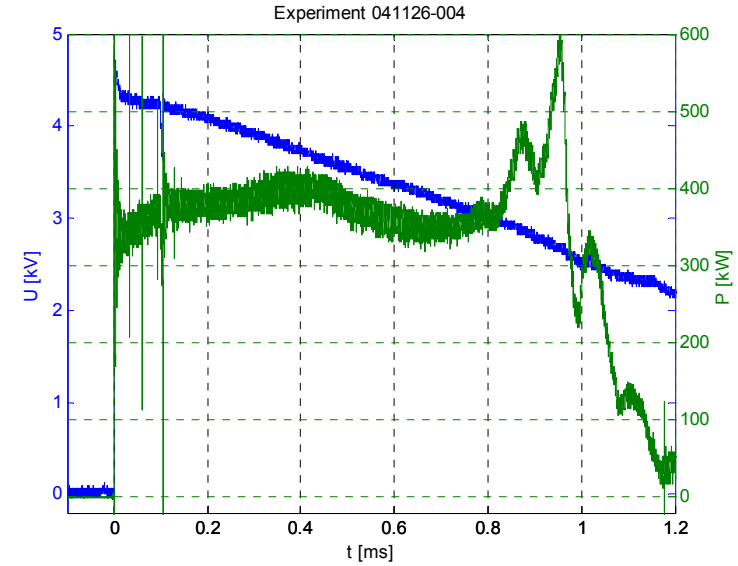

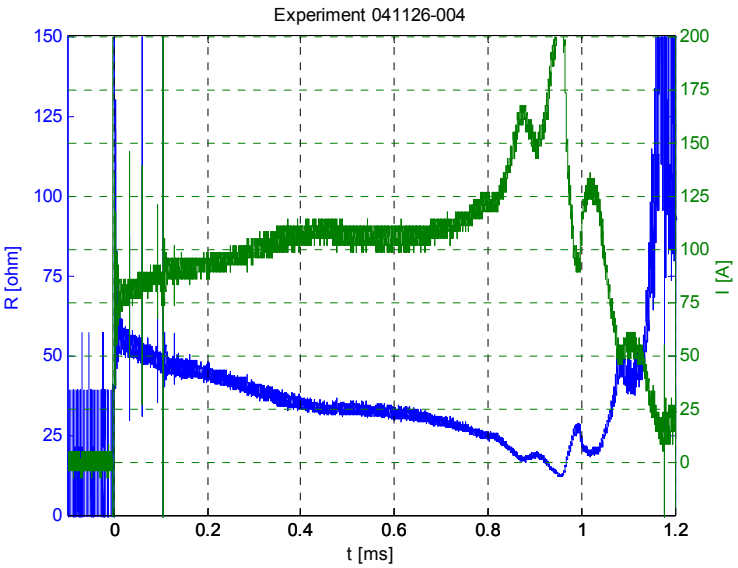

Experiment 041126-005

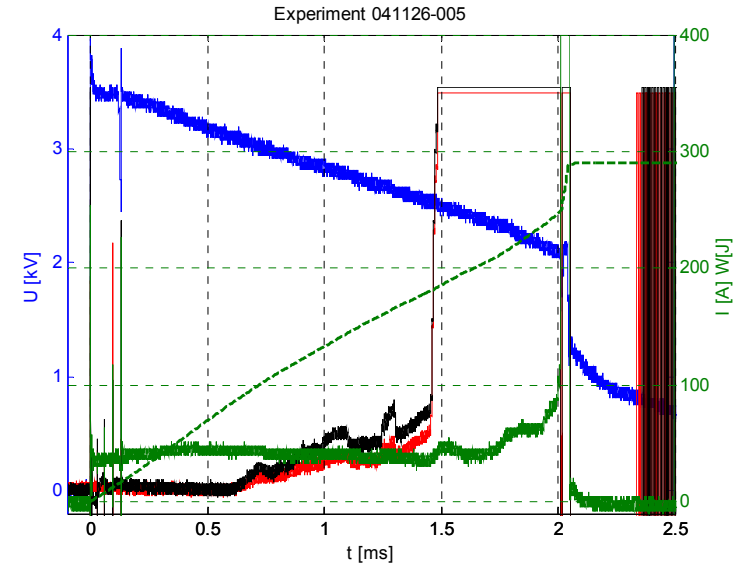

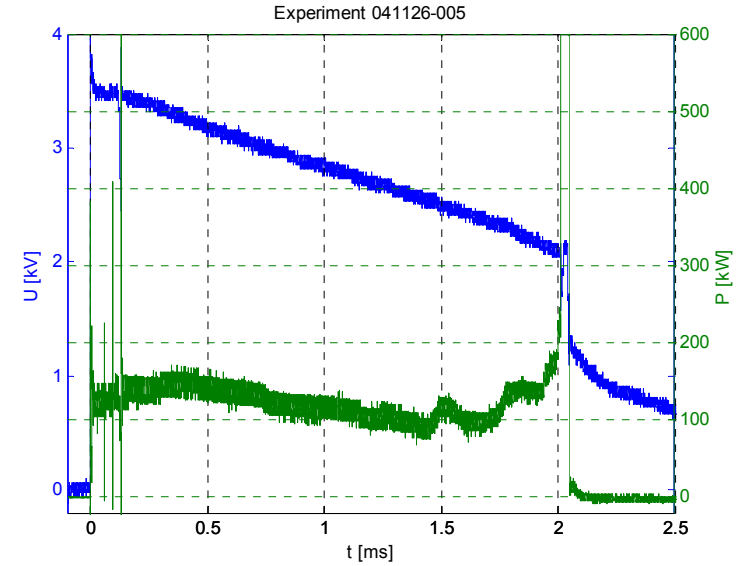

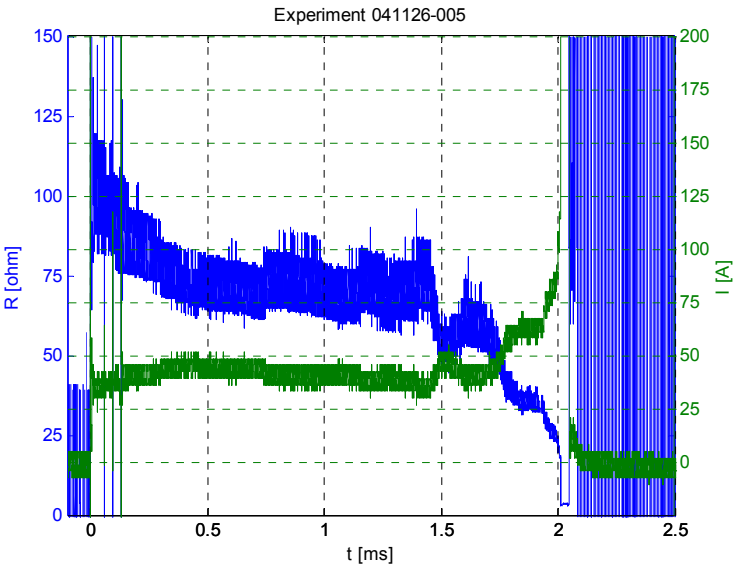

Experiment 041126-006

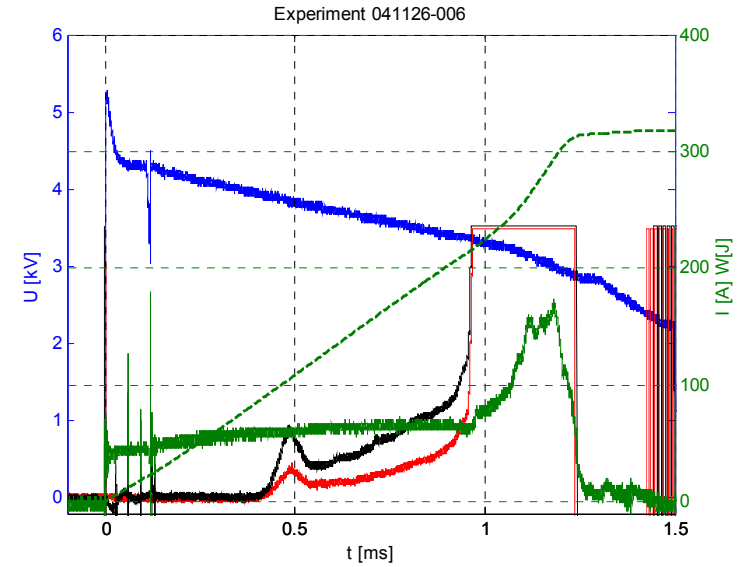

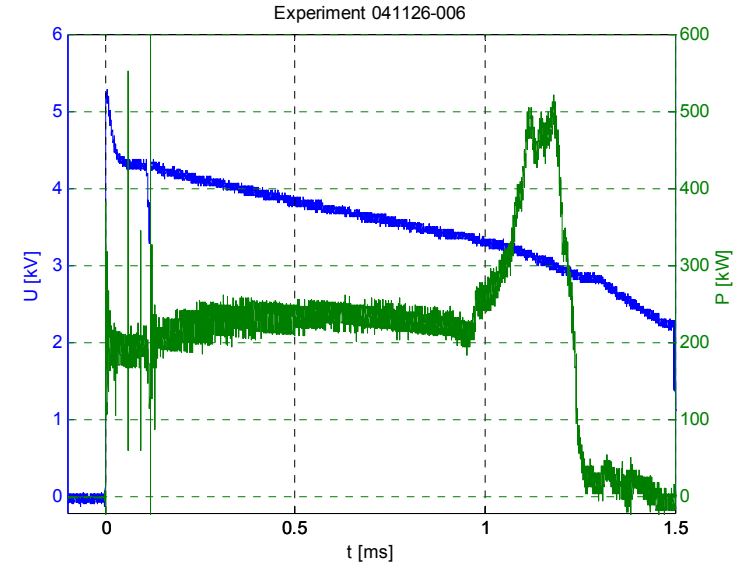

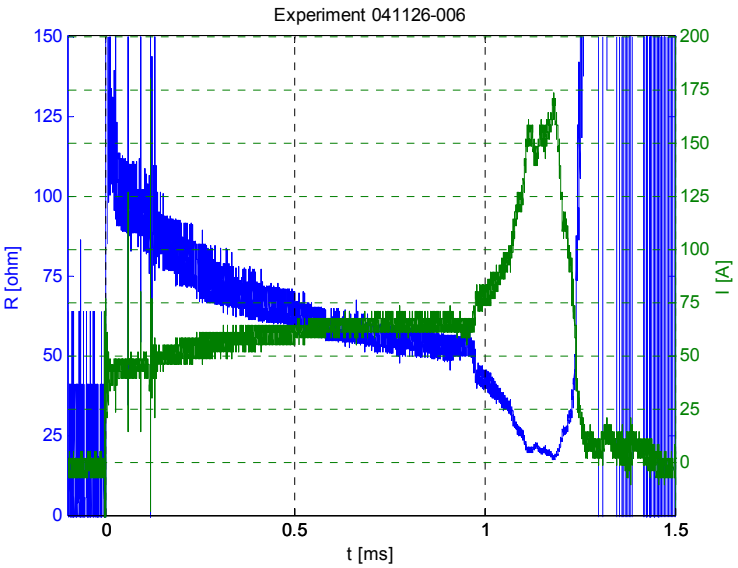

Experiment 041207-001

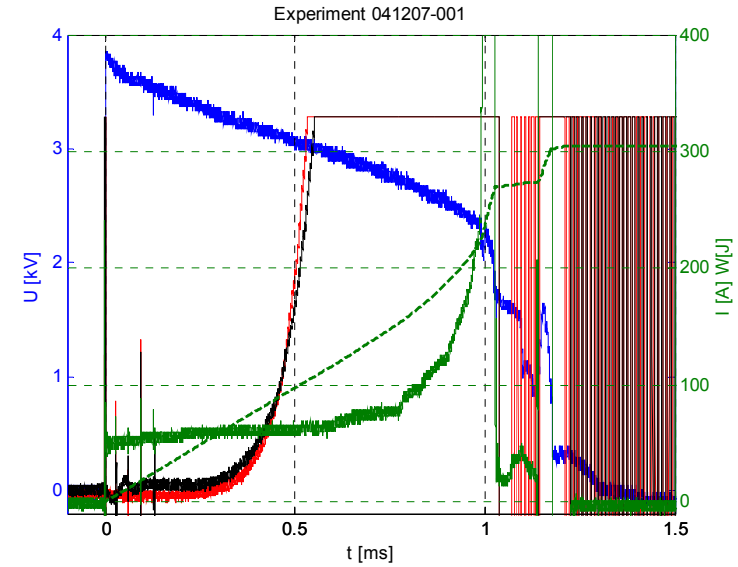

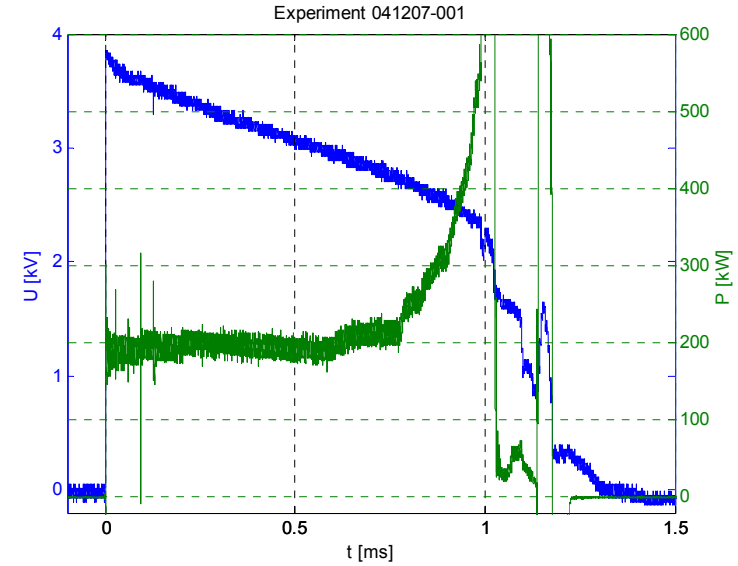

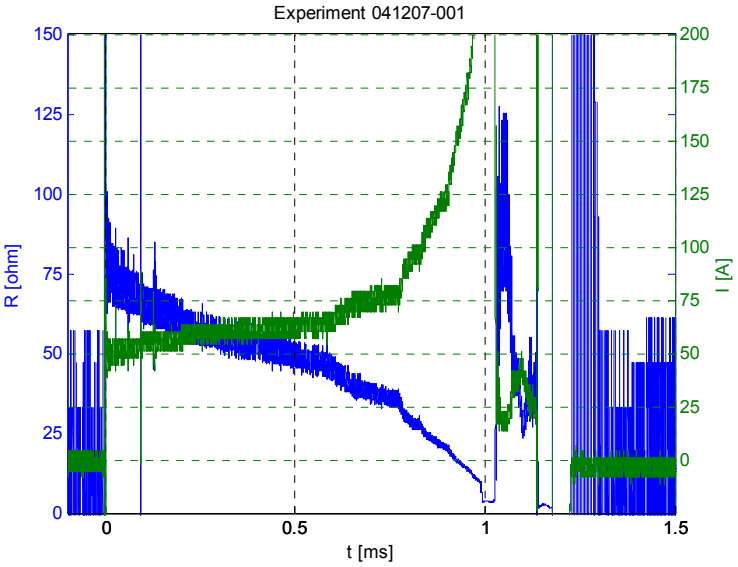

Experiment 041207-002

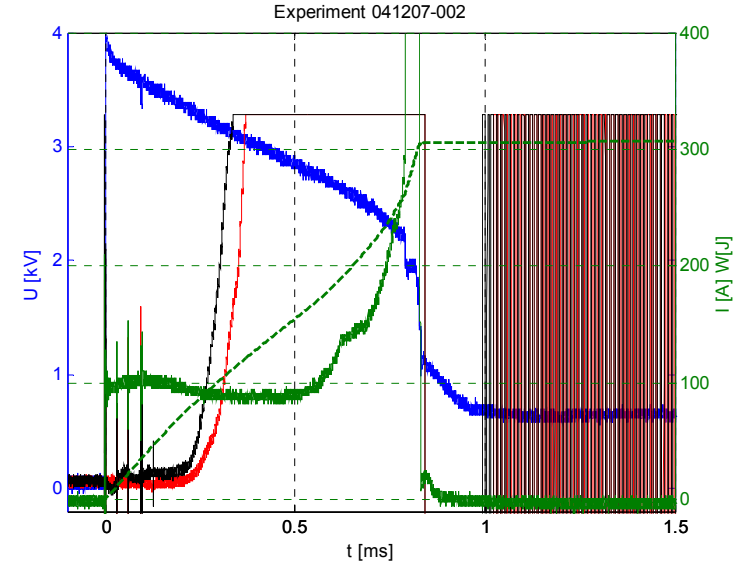

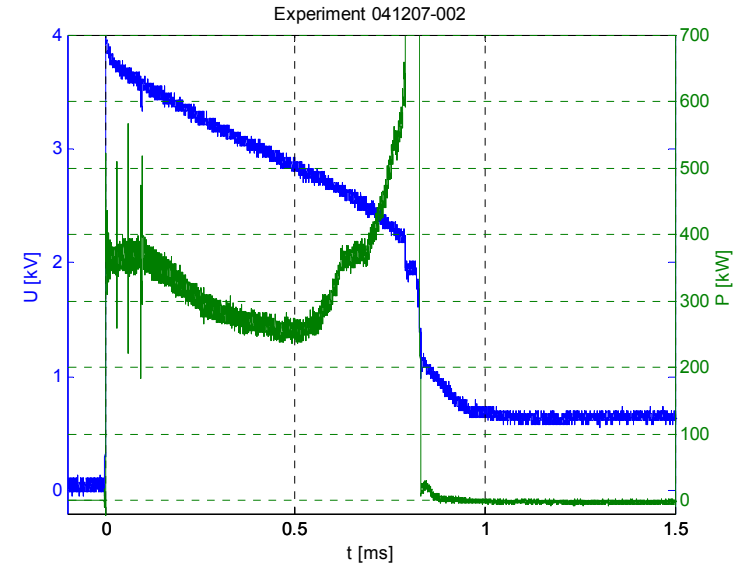

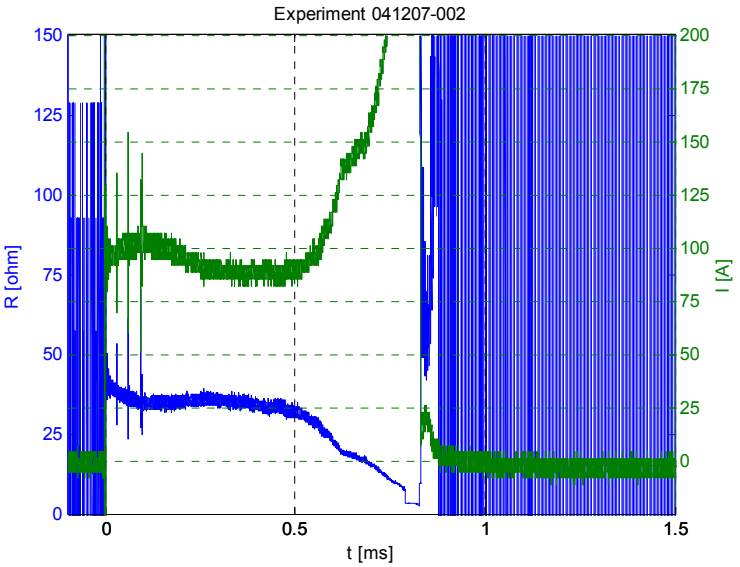

Experiment 041207-003

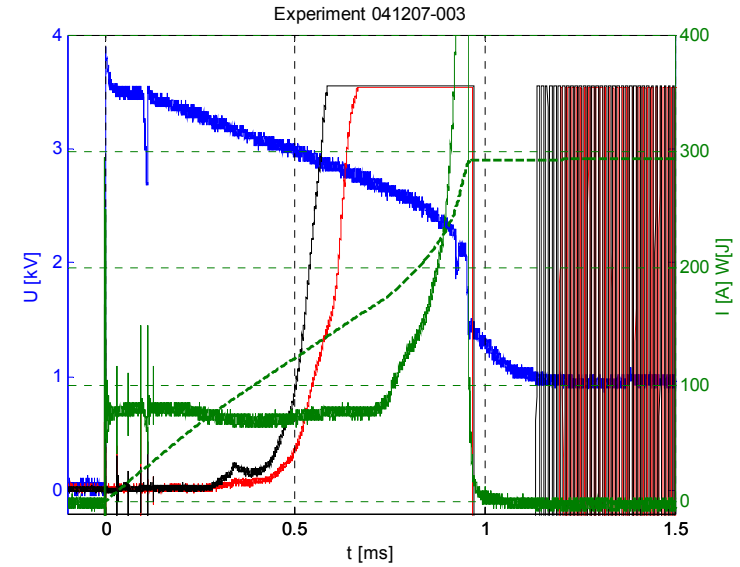

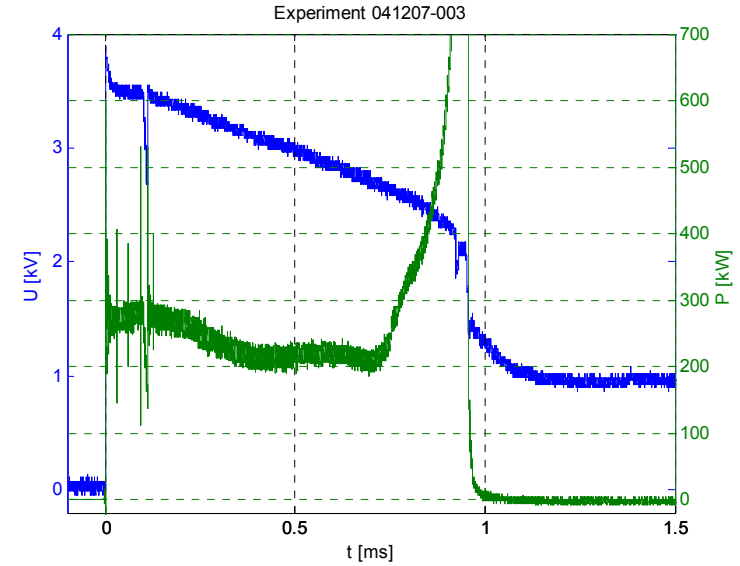

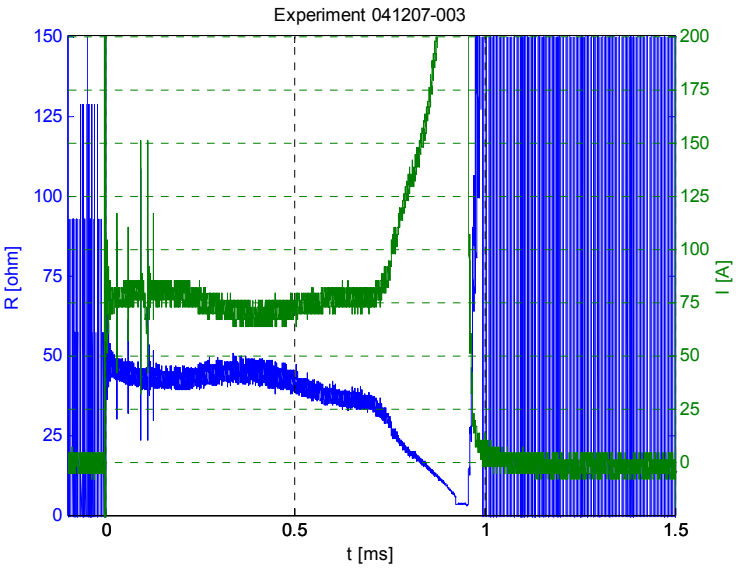

Experiment 041222-001

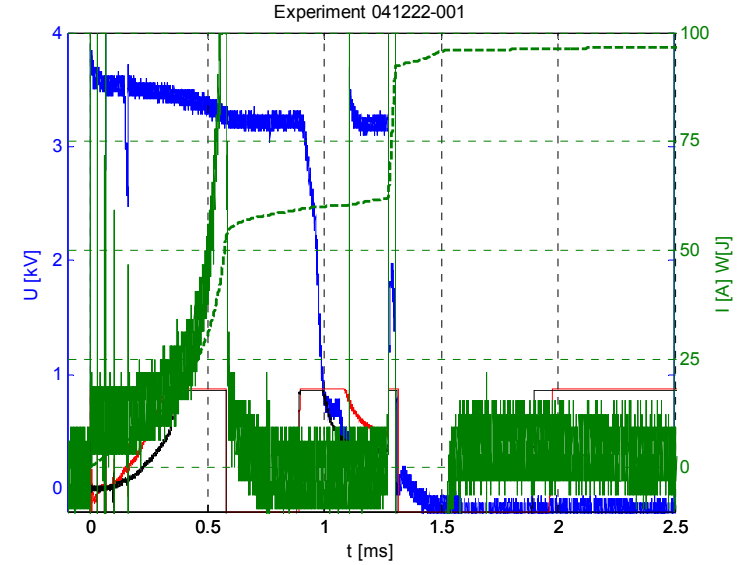

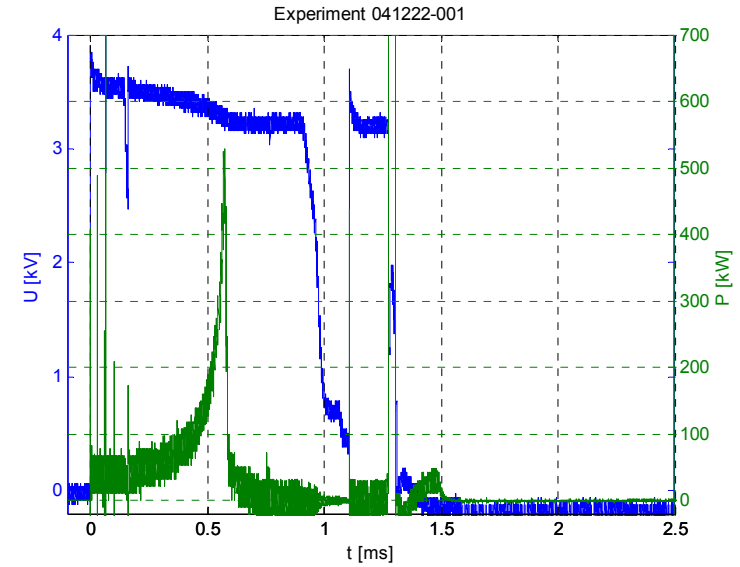

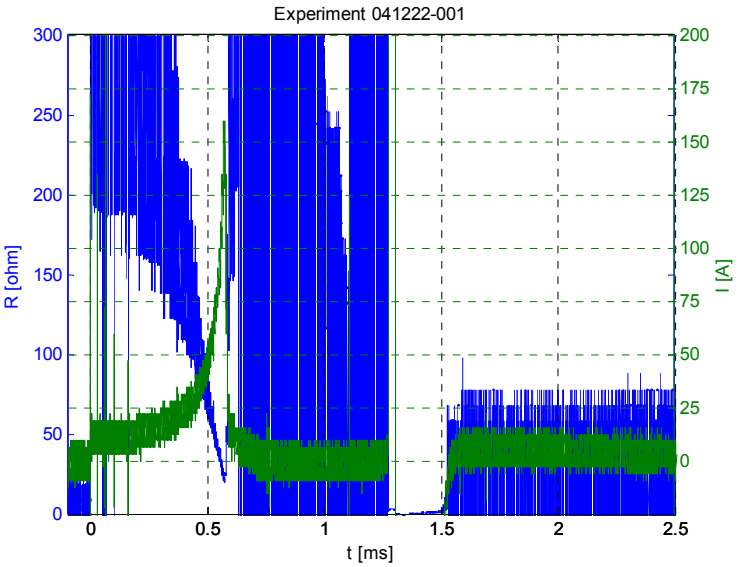

Experiment 041222-002